Deciphering the Drivers Favorable for Summer Monsoon Precipitation Extremes over the Indian Himalayas

Rohtash Saini[1] and Raju Attada[1,*]

[1]Department of Earth and Environmental Sciences

Indian Institute of Science Education and Research Mohali, Mohali, Punjab-140306

Submitted to

JGR-Atmospheres

***Corresponding author:**

Raju Attada

Department of Earth and Environmental Sciences,

Indian Institute of Science Education and Research Mohali, India.

Email: rajuattada@iisermohali.ac.in

Abstract

This study investigates the physical processes behind extreme precipitation events (EPEs) in the Himalayas, notorious for causing frequent floods and significant loss of life and property. Due to the presence of complex terrain, understanding the driving factors behind these EPEs has proven challenging. Here, we decipher the driving conditions responsible for the occurrence of EPEs in the western Himalayas (WH) for the period 1979 to 2020. Our findings provide compelling evidence for the role of large-scale circulation patterns and their associated dynamics and thermodynamics in instigating EPEs. The presence of distinct upper-tropospheric gyres flanking the WH, alongside a prominent zonal wave pattern, underscores the conducive atmospheric configuration during EPEs. This configuration promotes a southward extension of the trough, intensifying the convergence of moisture-laden winds from the adjoining seas, leading to substantial moisture availability for the EPEs. Moreover, the southward advancement of cyclonic vorticity further aids in northward moisture advection towards the region. At a regional scale, using moisture budget analysis, we find that vertical moisture advection plays a significant role, emphasizing the dominance of local dynamics driving these EPEs. Furthermore, the intensifying diabatic heating structure over the WH leads to intensified convection through stronger vertical motions, facilitating the development of deep convection. Our results also pinpoint the role of the shifting of the Intertropical Convergence Zone (ITCZ), strongly linked to the dynamics of convective clouds, resulting in changes in the intensity of EPEs over the WH. Additionally, Quasi-Resonance Amplification is linked with the most intensified/persistent EPEs over the Himalayas.

Keywords: Western Himalayas, Extreme Precipitation, Physical drivers, Arctic warming

1. Introduction

The Himalayas, as the world's highest mountain range, feature a unique topography and climate dynamics that exert a significant effect on weather and climate patterns across northern India and neighbouring regions downstream. The hydrological cycle is heavily dependent on the abundant rivers, which sustain millions of people in the north Himalayan region (Hegdahl et al., 2016; Immerzeel et al., 2009; Jain et al., 2017; Li et al., 2016; Vellore et al., 2016; Saini and Attada, 2023). The region's large-scale topography is important in shaping the monsoon characteristics either by thermal or mechanical forcing. The Himalayas, on the other hand, encounter a substantial challenge due to their high vulnerability to extreme precipitation events (EPEs), particularly during the Indian Summer Monsoon (ISM) season (June through September-JJAS). These EPEs can have devastating consequences, including flash floods, landslides, and the loss of human lives and property (e.g. Houze, 2014; Rasmussen and Houze, 2012; Kotal et al., 2014; Ranalkar et al., 2016; Singh et al., 2015; Nischal et al. 2024). The vulnerability of the region to such catastrophic events is a matter of great concern. The destructive consequences of EPEs during the ISM have been made clear through recent past events. For example, torrential rainfall in Uttarakhand in 2013 led to substantial economic damages surpassing 3.5 billion US dollars and a heart-breaking toll of more than 6,000 lives lost (Chevuturi and Dimri, 2016; Joseph et al., 2015; Ranalkar et al., 2016; Shen et al., 2017). In recent years, a multitude of disasters triggered by extreme precipitation have unfolded, underscoring the region's susceptibility to EPEs. These include the Leh flood in July 2010 (e.g. Houze, 2012; Rasmussen and Houze, 2012), the Chamoli river flood in Uttarakhand (July 2016), Bilaspur and Shimla flood in August 2019 (S. Singh & Lal Kansal, 2022), and the Jammu & Kashmir's Kishtwar district floods in July 2021 (Ahmad et al., 2023). In the years 2022 and 2023, occurrences within the context of the ISM have contributed to an expanding catalogue of rain-triggered calamities. Notable among these incidents are the Amarnath flood in Kashmir (Sain et al., 2022), the inundation of Chhoj panchayat and Malana villages in Kullu, Himachal Pradesh (HP), and the devastating Nainital and Uttarkashi floods in Uttarakhand (UK). These events have inflicted significant human and economic losses.

In recent decades, the Western Himalayas (WH) have witnessed a notable increase in the frequency and intensity of EPEs, as reported by (Bharti et al., 2016; Malik et al., 2016; Shekhar et al., 2017). The pronounced warming observed in the Himalayas compared to other regions of India has directly influenced EPEs, impacting atmospheric dynamics and contributing to the occurrence of EPEs (Das and Meher, 2019; Krishnan et al., 2019; Negi et al., 2021; Sabin et al., 2020; Saini et al., 2023). Considering the projected rise in both frequency and intensity of EPEs due to climate change, studying and comprehend the mechanisms underlying these EPEs in the WH is crucial which remain relatively unexplored and warrant comprehensive study.

Few research studies (Rasmussen and Houze, 2012; Bharti, 2015; Dimri et al., 2016) have investigated the fragile nature of the Himalayan region, which encompasses high mountain ranges and deep valleys, creates a unique environment for atmospheric processes to occur. The interaction of moist air masses with the mountains and the complex topography can lead to significant heterogeneity in the regional spatiotemporal distribution of precipitation and the formation of localized convective storms and heavy precipitation (Dahri et al., 2016; Priya et al., 2017; Roy et al., 2021). Some observational and numerical modelling works have explored the exceptional occurrence of EPEs in the WH region. However, the aforementioned studies are constrained by limited spatial coverage, often employing a case-by-case approach focusing on only a few stations. Some case studies have presented the probable causes of EPEs over the Himalayas (Chevuturi & Dimri, 2016; Dube et al., 2014; George & Kutty, 2021; Houze et al., 2017; Medina et al., 2010; Nandargi & Dhar, 2011; Ranalkar et al., 2016; Shrestha et al., 2015). EPEs are often associated with convection prompted by orographic lifting, whereby the rugged Himalayan terrain compels the condensation of moisture, leading to precipitation (Bhardwaj et al., 2019; Bohlinger et al., 2017; Houze, 2012; Martius et al., 2013; Vellore et al., 2016). Furthermore, research studies have identified moisture advection as a key mechanism behind EPEs in the Himalayan region (Hunt & Parker, 2016; Vellore et al., 2020). Moist air masses from the BoB and AS are transported into an area by prevailing winds, enhancing the low-layer moisture flux and convergence over the foothills of Himalayas (Bohlinger et al., 2017; Hunt et al., 2018b; Martius et al., 2013; Roy et al., 2021; Vellore et al., 2020). In addition, the presence of warm and moist low-level air masses is constrained by a dry continental air mass originating from Afghanistan and the Tibetan plateau (Karki et al., 2018a). This vertical capping, along with horizontal obstruction by the mountain barriers of the foothills of the Himalayas, effectively impedes the premature release of convective available potential energy. This atmospheric configuration prevents the destabilization of the atmospheric stratification, thereby initiating the occurrence of extreme convective precipitation events (Houze, 2012; Karki et al., 2018b; Kotal et al., 2014; Kumar et al., 2014)

The rise in moisture triggers various microphysical processes, resulting in the formation of hydrometeors and the development of deep clouds in the region (S. Das et al., 2006; Hazra et al., 2016; Schomburg et al., 2012).Therefore, moisture advection leads to the formation of persistent precipitation events, which can result in flooding and landslides over the Himalayas (Chaudhuri et al., 2015; Jiang et al., 2014). Furthermore, study Vellore et al., (2016) attempts to explain monsoon-extratropical circulation interactions across the Himalayas.

Although a few case-based studies have shed light on the significant impacts of EPEs over the Himalayan region, there is still much unknown about their underlying large-scale drivers and its associated mechanisms. The existence of knowledge gaps pertaining to the primary drivers causing the EPEs and improving the understanding of how large scales factors along with localised and synoptic factors responsible for EPEs necessitates further in-depth investigations. Therefore, conducting research in this area is crucial to better comprehending the contributing factors to EPEs and developing effective strategies for mitigating their adverse impacts. We aim to address the following major objectives that are (a) to explore the distribution of EPEs over the WH during ISM, and (b) to investigate the synoptic and large-scale drivers of EPEs over the Himalayas and exploring the dynamic and thermodynamic responses. The study objectively characterizes the composite anomaly of precipitation-related variables of EPEs at the near-surface and upper troposphere. Finally, the present study will better understand the complex interactions between the large-scale factor and regional weather patterns and inform strategies for building climate resilience in the Himalayan region. It will help shed light on the mechanisms and factors contributing to EPEs.

The remainder of the paper is as follows: Section 2 provides an overview of the data and methodology employed in this study. In Section 3, we delve into the synoptic conditions during EPEs, elucidating the associated dynamic and thermodynamic responses. Additionally, this section explains the moisture and heat budget, concurrently investigating cloud microphysical characteristics. Lastly, it explores the role of Quasi Resonance Amplification (QRA) in EPEs over the Himalayas. Section 4 encapsulates the study's findings, presenting a summary and drawing conclusions.

2. Data and Methodology

2.1 Study area

The study area lies in the northern part of the Himalayan range, spanning from 25.5° N to 37.5° N and 72° E to 86° E (outlined in Fig. 1a), comprised of the foothills of the Himalayan range, the Shivalik ranges, and the Siwalik Hills. The elevation of the study varies hundreds of meters from sea level to more than 7000 meters as shown in Figure 1(a) and foothills of Himalayas are outlined with the blue rectangular box. The magenta color contour shows the topographic complexity of the WH surpassing the 60 percent mark on the 0 to 100 scale. It indicates a significantly higher level of topographical intricacy, signifying the region as severe and complex compared to the global average. The region's climate system is highly diverse, encompassing a wide range of factors that influence precipitation distribution and extreme weather events. Understanding the dynamics of the foothill of Himalayas is essential for unraveling the intricate climatic patterns within the broader WH region.

2.2. Data used

We used ERA5 dataset, which is a comprehensive and high-resolution fifth-generation reanalysis dataset developed by the European Centre for Medium-Range Weather Forecasts (ECMWF). It provides extensive and detailed data with a spatial resolution of 0.25°×0.25° (Hersbach & Dee, 2016). ERA5 is generated using an advanced 4D-Var assimilation system that incorporates multiple sources of data such as surface observations, weather station measurements, satellite data, and weather radar information (Hersbach & Dee, 2016). In the present study we have used daily ERA5 data spanning from 1979 to 2020 to investigate the EPEs throughout the ISM using composite analysis approach. We have focused on various atmospheric variables, such as surface pressure, 2-meter air temperature, vertical pressure velocity, geopotential height, horizontal wind components. ERA5 data is used to derive dynamic and thermodynamic variables like moist static energy (MSE), Ertel potential vorticity (EPV), and vertically integrated moisture transport (VIMT), were obtained from the ERA5 dataset. We also used the same dataset to examine the cloud microphysical properties such as total column cloud ice, snow water, ice water and supercooled liquid water during summer monsoon EPEs over Himalayas. We used soil moisture and topography complexity data from the ESA CCI Soil moisture climate change initiative. The detailed description is available on the website (http://www.esa-soilmoisture-cci.org/node/139) for the data. We have also used the gridded daily rainfall data IMD, regional reanalysis dataset – Indian Monsoon Data Assimilation and Analysis (IMDAA), and satellite-based datasets Integrated Multi-satellite Retrievals (V3) for Global Precipitation Measurement (GPM-IMERG), a merged high-resolution satellite product for detecting the EPEs over WH.

2.3. Methodology

In this study, EPEs are identified using the percentile approach during ISM over the WH, with EPEs defined as instances where precipitation exceeds the 99th percentile. So far, there has yet to be an established standard definition for EPEs as it depends on the region of interest and its severity. Notably, the IMD employs a threshold value to categorize various levels of rainfall, ranging from light to extremely heavy. However, due to the diverse nature of the Himalayas, encompassing heterogeneity, varied terrains, and overall complexity, the common practice for defining precipitation extremes in this region involves the use of percentile thresholds (Bharti et al., 2016; Nischal et al., 2023, 2024). The threshold is selected based on the potential impact of cumulative precipitation above this level across all grid points within the region, which can lead to downstream flooding and landslides, affecting crops in the study area (Hunt et al., 2018b). To ensure consistency, the precipitation dataset is re-gridded to match the resolution of the ERA5 dataset (0.25° × 0.25°). This study uses the Mann-Kendal (Mann 1945; Kendall 1948) for trend detection. The M-K test is a rank-based non-parametric based method and is usually used in hydrometeorological time series (Wang et al., 2020).

Furthermore, this study delves into the role of large-scale circulation in EPEs. It unveils synoptic features and atmospheric circulation patterns linked to EPES in the Western Hemisphere (WH) through the examination of composite anomalies of atmospheric variables associated with precipitation. EPEs are obtained from an IMD gridded precipitation dataset over the foothills of Himalayas. To obtain insights into the fundamental physical mechanisms driving changes in EPEs, a composite map is generated by subtracting the average conditions of non-extreme days from those of extreme days, spanning the period from 1979 to 2020. Additionally, the study investigates the dynamic and thermodynamic aspects of EPEs, as they provide valuable information about the atmospheric conditions associated with EPEs.

Vertical Integrated Moisture Transport (VIMT): VIMT measures the total amount of moisture in the atmosphere that is moved up or down within a vertical column of air (Zhang et al., 2001). It is an essential metric for understanding the atmospheric dynamics of weather, climate, and water resources (Chansaengkrachang et al., 2018; Fasullo & Webster, 2003; Ullah & Shouting, 2013). The following equation (1) is used to calculate the VIMT.

$$VIMT = -\frac{1}{g}\int_{1000\,hPa}^{300\,hPa} q\left(\frac{du}{dx} + \frac{dv}{dy}\right)dp \ldots\ldots\ldots\ldots\ldots\ldots..(1)$$

g represents the gravitational acceleration, *q* indicates specific humidity, and *u* and *v* zonal and meridional velocity, respectively. VIMT is obtained by vertically integrating moisture fluxes of the u and v in pressure level from surface to 300hPa, as shown in equation (1).

Moist Static Energy (MSE): MSE serves as a thermodynamic parameter that provides insight into the energy content of moist air present in the atmosphere. It considers the latent heat released during the condensation of water vapor in the parcel into liquid or solid precipitation, as well as the potential energy related to the parcel's height (Andersen & Kuang, 2012; Dube et al., 2014). This definition highlights the fundamental principles of conservation applicable during moist adiabatic processes and within a state of hydrostatic (Dube et al., 2014; Maloney, 2009). Within a stable, any variations in gravitational potential energy find equilibrium through corresponding changes in enthalpy due to pressure fluctuations. An increase in MSEs integrated into a column means importing MSEs from the environment. This destabilizes the atmospheric column through heating and humidification processes, which are then induced by deep convective precipitation. Conversely, the decline in column integrated MSE suggests tropospheric stabilization due to cooling and drying mechanisms, resulting in the export of MSE to the affected regions. Under the standard approximation, MSE (value per total air mass) is defined by equation (2).

$$MSE = C_P T + gz + L_v q \ldots\ldots\ldots\ldots\ldots\ldots\ldots\ldots\ldots (2)$$

where C_P is specific heat capacity at constant pressure (1004 J kg^{-1} K^{-1}), T denotes the air temperature, g represents the gravitational acceleration (9.8 m s^{-2}), z is the geopotential height, L_v is the latent heat of vaporization, and q is the specific humidity. In the equation (2), the first term corresponds to dry-air enthalpy (or heat content), the second term represents specific gravitational potential energy, and the last terms potentially contribution to the first term due to latent heating.

Moisture Budget: The study emphasized the crucial role of ample moisture availability in order to generate high precipitation amounts, employing a moisture budget analysis. To evaluate the individual components of the moisture budget, we used daily measurements of total precipitation, specific humidity, omega, and the u and v components of winds at various levels spanning from the surface to the troposphere. Employing the vertically-integrated water budget methodology at a daily temporal scale enables us to dissect and thoroughly investigate the distinct facets contributing to precipitation extreme (Oueslati et al., 2019; Sudharsan et al., 2020). In accordance with the vertically-integrated water budget, precipitation can deconstructed as equation (3) (Trenberth, K.E., Houghton, J.T. & Filho, 1995; Trenberth & Guillemot, 1998)

$$P = E - \frac{1}{g}\int_0^p \omega \frac{\partial q}{\partial p} - \frac{1}{g}\int_0^p V\nabla q - \frac{1}{g}\int_0^p \frac{\partial q}{\partial t} \ldots\ldots\ldots..3$$

In the given equation (3), E (mm/day) denotes evaporation, ω (Pa/day) represents the vertical velocity, V (m/day) stands for horizontal wind, q (kg/kg) indicates specific humidity, and p(Pa) denotes atmospheric pressure. This equation can alternatively be expressed as

$$P = E + V_{adv} + H_{adv} - \partial_t q \ldots\ldots\ldots..4$$

As the contribution of $\partial_t q$, to the moisture budget in equation 4 is usually negligible compared to the other terms, we can omit $\partial_t q$, and rewrite it as equation (5)

$$\mathrm{P} = \mathrm{E} + \mathrm{V_{adv}} + \mathrm{H_{adv}} \ldots\ldots\ldots..5$$

where, V_{adv}, H_{adv} and $\partial_t q$ denotes the vertical moisture advection, the horizontal moisture advection, and the time derivative of q, respectively. Further, the vertical moisture advection is decomposed by

$$\mathrm{V_{adv}} = \mathrm{Dynamic} + \mathrm{Thermodynamic}$$

$$\mathrm{V_{adv}} = -\left[\frac{1}{g}\int_0^p \Delta\omega \overline{\frac{\partial q}{\partial p}}\right] - \left[\frac{1}{g}\int_0^p \overline{\omega}\Delta \frac{\partial q}{\partial p}\right] \ldots\ldots\ldots..6$$

The dynamic component in vertical moisture advection corresponds to the changes in vertical velocity during the EPEs, while the thermodynamic component primarily pertains to alterations in atmospheric water vapor, aligning with the concept of the Clausius-Clapeyron equation. (Allen & Ingram, 2002; Pall et al., 2007; Pfahl et al., 2017).

Estimation of Apparent Heat Source (Q1) and Moisture Sink (Q2): This study presents the computations of diabatic heating over the Himalayas in terms of apparent heat source (Q1) and apparent moisture sink (Q2). The studies by (Yanai, 1961; Johnson, 1987; Yanai and Tomita, 1998) which have also been utilized in other research works (Attada et al., 2020; Mukhopadhyay et al., 2010) underscores the significance of vertical heating distribution in driving monsoon circulation and contributing to substantial rainfall amounts. We calculated the apparent heat source (Q1) and apparent moisture sink (Q2), along with their vertical integrations within an air column following (Yanai & Tomita, 1998). The expressions for Q1 (equation 7) and Q2 are (equation 9)

$$\mathrm{Q_1} = \mathrm{C_p}\left(\frac{\mathrm{P}}{\mathrm{P_0}}\right)^{k}\left(\frac{\partial\theta}{\partial t} + \mathrm{V}.\nabla\theta + \omega\frac{\partial\theta}{\partial \mathrm{P}}\right) \ldots\ldots\ldots..7$$

$$\mathrm{k} = \frac{\mathrm{R}}{\mathrm{C_p}} \ldots\ldots\ldots..8$$

and

$$Q_2 = L\left(\frac{\partial q}{\partial t} + V.\nabla q + \omega\frac{\partial q}{\partial P}\right) \ldots\ldots\ldots..9$$

where θ represents the potential temperature, q signifies the specific humidity, denotes the horizontal velocity, ω stands the vertical velocity, and p indicates the pressure in equation 7. R and C_p are the gas constant and the specific heat at constant pressure, respectively. Q1 is determined by combining the latent heating linked to phase changes, vertical eddy transport, surface sensible heat flux, and radiative heating. Likewise, Q2 consists of net condensation, vertical eddy transport of moisture, and subgrid mixing (Liu and Moncrieff., 2007). The heating profiles are significantly influenced by microphysical phenomena such as evaporation and condensation, as demonstrated by (Rajeevan et al., 2010; Rogers et al., 2007) in their studies. These processes, in turn, hinge on the hydrometeor mixing ratios specified within different microphysics schemes. We have expanded our investigation to explore the presence and behaviour of hydrometeors within the atmosphere, aiming to enhance our comprehension and predictive capabilities related EPEs. Several studies (Hazra et al., 2016; Luo et al., 2009) revealed that alterations in cloud microphysical properties can have an effect on mesoscale dynamics of any extreme event, as hydrometeors size, shape, and density can impact how they interact with other particles and with the atmospheric environment, which, in turn, affects the formation and intensity of precipitation. Therefore, we have investigated the composite anomaly of hydrometeors (total column of total column cloud liquid water, total column cloud ice water, total column snow water, total column supercooled liquid water, and total column water vapour. We further investigated the extratropical influences and the dynamical and thermodynamical characteristics of the synoptic condition's setup prior to the EPEs over the Himalayas.

Ertel Potential Vorticity (EPV): EPV is calculated to investigate the extratropical influences in triggering extreme precipitation events over the Himalayas. It is particularly important to understand the dynamics of upper-level troughs and ridges, which are crucial in developing and stirring weather systems (Raju et al., 2015; Sandhya et al., 2015). Extreme precipitation and flood events in the Himalayas are frequently linked to synoptic condition characterized by interactions between equatorward moving upper-level extratropical circulations and moisture-rich tropical monsoon circulation. Therefore, this study calculated composite anomaly EPV (PV; on the 350 K surface) to analyze the extratropical interaction over the heavy rainfall region HFR. IPV is formulated by following the equations.

$$P = -g(\zeta_\theta + f\ )\frac{d\theta}{dp} \dots\dots\dots\dots\dots\dots\dots\dots (10a)$$

$$\zeta_\theta = -\left(\frac{\partial v}{\partial x} + \frac{\partial u}{\partial y}\right)_\theta \dots\dots\dots\dots\dots\dots\dots .. 10(b)$$

Here P is the isentropic potential vorticity (or Ertel's PV), ζ_θ is relative vorticity calculated on the isentropic surface, f is earth's vorticity (latitude dependent), $\frac{d\theta}{dp}$ Lapse rate of potential temperature. IPV is denoted in potential vorticity unit (P.V.U.) where for synoptic scale motions 1PVU is equal to 10^{-6} m^2 s^{-1} K kg^{-1}.

3. Result and Discussions

This section presents the synoptic conditions responsible for the occurrence of EPEs over the WH. Furthermore, this section interprets the dynamic and thermodynamic feedback mechanisms that play a role in the genesis of EPEs in the Himalayan region.

3.1 Synoptic dynamics of EPEs

We investigate the composite anomalies of precipitation, total precipitable water, outgoing longwave radiation (OLR), 2-meter air temperature and soil moisture to explore the associated atmospheric variables for precipitation events that trigger EPEs in WH. The most copious amount precipitation (exceed 35 mm day^{-1}) is noticeable in the vicinity of foothills of the Himalayas as shown in Figure 2a. This geographical distribution of the EPEs implies that extreme precipitation in the foothills of the Himalayas exhibits regional consistency, indicating that these events could be modulated by large-scale circulation along being localized drivers. In addition, positive anomalies of total precipitable water are clearly seen over the foothills of Himalayas, showing enhanced atmospheric moisture content during extreme events contributing to excess precipitation (Figure 2b). It is to be noted that extreme precipitation amounts are usually proportional to precipitable water (e.g. Ccoica-López et al., 2019; Kunkel et al., 2020). This excess moisture aids for producing more precipitation and, thereby, provides conducive environment for the occurrence and persistence of extreme precipitation in the Himalayas. Furthermore, composites of OLR (Figure 2c) anomalies during EPEs exhibits lower OLR values is covered over the WH region, and intensified more along with foothills of Himalayas, highlighting the presence of deep convective activity in the region. It is noteworthy that the convection is triggered by the forcing of monsoon winds over the topography. This extreme rainfall induces a significant surface cooling in the Himalayan foothills and its adjacent regions as shown in Figure 2d. This process cools the surface and warms the atmosphere, where water vapor condenses and releases heat in the mid-troposphere. In addition, the positive anomaly of soil moisture (Figure 2d) indicate that higher soil moisture is available for the precipitation region. As the lower tropospheric monsoon flow advances the Himalayan foothills, it encounters significant surface heat flux, primarily driven by evaporation and evapotranspiration processes (Figure S1). Consequently, by the time it reaches the Himalayas, this flow becomes saturated with moisture and becomes highly prone to potential instability.

This soil-precipitation feedback helps in increasing atmospheric moisture which leads to more precipitation which further saturates soil and lower the surface temperature.

3.1.1 Dynamical Characteristics

The spatial distributions of upper (200hPa) tropospheric geopotential height composite anomalies (Figure 3a) depicts an anomalous low-pressure system is formed over the northern Himalayan region and its vicinity, whereas two high-pressure systems are observed over the western (Eurasia) and eastern (Tibetan) peripheries of the WH during EPEs. Notably, the Eurasia high, northwestern Himalayan low pressure and Tibetan high form a characteristic wave-like pattern with canters of alternating polarities extending across the northwest India belt. The wave-like pattern (zonal wave) position at 500hPa shows strong equatorward protrusion of the westerly trough over WH, suggesting a baroclinic feature, leads to atmospheric instability that trigger the extreme precipitation. The dynamical mechanism driving the equatorward extension of the midlatitude westerly trough into the WH region involve a blocking high situated over western Eurasia and a Tibetan high on its east (Figure 3a). This configuration induces a robust anomalous south-westerly airflow from the Arabian Sea toward the WH region. The equatorward movement of the low trough also aligned with the cyclonic vorticity (details shown in the result section 3.4). In addition, the vertical pressure velocity at 500hPa has been shown in (Figure 3b) during ISM over the Himalayas. The large-scale vertical pressure velocity during the ISM regime represents the strong ascent of moist air parcel at 500hPa that prevails over the WH along with a gigantic plain region, and its manifestation can be seen in the dominance of EPEs of cloud burst nature (Vellore et al., 2020). In addition, the combination of elevated moisture levels, orography, and midlatitude diabatic heating results in high-pressure vertical velocity. This facilitates the ascent of moisture to higher altitudes, where it releases latent heat, thereby initiating deep convection over the Himalayas. Regarding EPEs, the areas with significant vertical motion align consistently with the regions of intense precipitation, as illustrated in (Figure 2a). Overall, from the EPEs composite analysis, study highlights the predominant role of vertical velocity in triggering extreme precipitation. Finally, the wind composites over the WH region shown in Figure 3(c, d). The lower tropospheric anomalous circulations show stronger south-westerlies (southeasterlies) over the AS (BoB), merging along the foothills of the Himalayas Figure 3(c). It is clearly noticed that the south-westerly wind from the AS dominates more than the southeasterly flow BoB and is directed and intensifying towards the WH region during heavy rainfall episodes. In addition, the positive anomaly of low-level relative vorticity (shown in yellow contours) aligns with an intensified cyclonic circulation pattern over the Himalayas during EPEs. The presence of anomalous low-level cyclonic vorticity over western India and the lower altitude areas of the Himalayan foothills creates favourable conditions for wind convergence towards the WH. Upper-level wind composite anomalies shown in Figure 3(d) exhibit cyclonic circulation over the Hindu Kush Mountainous region and anticyclonic flow over Tibetan, which couple to generate strong cyclonic-anticyclonic pairs of gyres (west and east sides of the study region). Interestingly the point of interaction of the pairs of gyres of cyclonic-anticyclonic are observed over the northern flank of the Himalayas and make the favourable condition divergence of wind at the upper levels (200hPa), thereby enhancing the low-level meridional winds poleward of the WH region. As the moist air masses approach the Himalayas, they are orographically lifted, finally triggering convection (Houze, 2014; Medina et al., 2010; Paula Barros & Lettenmaier, 1994). These circulation patterns provide favourable dynamical conditions for the occurrence of extreme summer precipitation events over the WH. In addition, mass stream function has been used to understand role of ITCZ location during the EPEs over WH. According to the Byrne and Schneider, 2016 location of the ITCZ is defined as the latitude nearest to the equator where the zonal mean stream function, average vertically between 700 and 300hPa, equals zero. Figure 3 (e) shows the zonal mean stream function area averaged over the longitudinal range of 70°E to 100°E in yellow line for non-extreme days and in magenta line for extreme days. Our results indicate that the ITCZ is located at 33.1°N during the non-extreme days, while it shifts by 2.49°N to the north during the extreme days. This shift is significant as it can enhance the precipitation amounts in the WH, potentially causing localized flooding. Our findings are also consistent with those of Kad and Ha, 2023, underscoring the influence of ITCZ in wet years. These research findings underscore the significant impact of large-scale dynamics on shaping the local atmospheric thermodynamic conditions over the WH during EPEs.

Based on the above analyses, it has been found that the zonal wave pattern over the mid and upper troposphere. Notably, the western Siberian High, western trough, and the Tibetan high are identified as profound weather systems during EPEs. These deep weather systems significantly influence the vertical structure of the atmosphere. Therefore, examining the atmospheric vertical structures associated with EPEs during the ISM is crucial. Figure 4 displays the composite vertical-meridional and vertical- zonal cross-sections of geopotential height and vertical pressure velocity anomalies along the longitude spanning from 30° E to 120° E, and latitude spanning 22° N to 38° N respectively. As depicted in Figure 4a, negative anomalies in the geopotential height field span the entire troposphere (from the surface to 300hPa) around 72°E, extending eastward over the Himalayan range, and it has the strongest anomaly up to 30 m at around mid-troposphere (500hPa). This anomalous baroclinic structure, with stronger responses observed at 500hPa, implies the influential role of the upper-tropospheric circulation associated with the anomalous wave pattern. These results are consistent with the result shown in Figure 4(a). Collectively Figures 3a and Figure 4a suggest that the deep western trough characterizes the EPEs during ISM over the Himalayas, with two highs, the Siberian high and the Tibetan high. We also notice in Figure 4b high negative pressure velocity in the mid-troposphere around 72°- 80°E suggesting an ascending air column that spans the entire troposphere over the Himalayan region, which causes strong convective activities, therefore, more cloud formation and heavy precipitation. In addition, vertical-zonal cross-sections of geopotential height and vertical velocity along the latitude spanning from 20N° to 38°N, are shown in Figure 4 (c, d) respectively. Finding exhibits the cyclonic features at lower tropospheric and anticyclonic feature at upper tropospheric level that promote the lifting of warm, moist air and trigger the development of EPEs. Result also shows north-south strong mid tropospheric low-pressure gradient and high negative pressure velocity in the mid-troposphere around 28°- 32°N indicating ascending air column over the WH. Overall, the vertical structure of geopotential height and vertical pressure velocity contribute to favourable dynamical conditions for the occurrence of extreme precipitation over the WH. Furthermore, Figure S2 presents a display of vertical-meridional cross-sections showing anomalous wind components along the meridian 72º-80ºE. The results notably show an increase in meridional winds along with significant mid-tropospheric vertical motion has been observed shown in (Figure S2) over the Himalayan foothill region. The convergence in the foothill region coincides with enhanced convergence extending up to 400hPa at high elevations within the study region. Simultaneously, upper-level divergence evidently contributes to the acceleration of the upper-level jet.

3.1.2 Thermodynamical characteristics

Atmospheric moisture is a major contributor to EPEs, so investigating extreme precipitation requires monitoring its changes and sources of moisture. Thus, moisture transport analysis provides insight into the dominant modes of precipitation variability as well as the moisture sources feeding the EPEs over the Himalayas. A composite analysis was carried out to study moisture sources and moisture transport via VIMT in the atmospheric column from 1000 to 300hPa, with vectors depicting the direction of moisture transport shown in Figure 5a. The findings show that moisture transport appears from the southwest and southeast of the study area towards WH from the AS and BoB during the EPEs. Strong moisture with moisture components from the AS and BoB towards WH is carried by a south-westerly wind and southeasterly winds during the EPEs. The Positive anomaly of VIMT provides clear evidence of available moisture over WH, which helped form the intense convective system and resulted in a severe storm over the Himalayan region. Previous studies (Aggarwal et al., 2021; Chevuturi & Dimri, 2016; Karki et al., 2018b) also found that anomalous high moisture incursions from the AS and BoB along with monsoon troughs are the significant contributor for moisture sources generates precipitation over the foothills of the western Himalayas. In addition, the analysis reveals a notable feature in the lower Himalayan foothill belt, where there is a significant positive anomaly in Convective Available Potential Energy (CAPE) and an intense negative anomaly in Convective Inhibition (CIN) shown in Figure 5b. CAPE representing atmospheric instability, indicates the potential energy available for convection, while CIN quantifies the energy required to overcome stability and initiate deep moist convection. The finding indicates heightened atmospheric instability and reduced inhibition, facilitating the increase in available parcel energy. Consequently, the increase in CAPE fosters strong moist convection, thunderstorms, and ultimately leads to EPEs in the region.

Further analysis of the MSE was carried out to study the large-scale climatic influences on EPEs as depicted in Figure 5c. MSE mainly signifies a thermodynamic indicator of the atmospheric column. An increase in MSE signifies the influx of MSE from the surrounding environment, which destabilizes the atmospheric column through heating and moistening processes (Maloney, 2009; Zheng et al., 2020). The finding highlights an anomalously strong MSE build-up within the mid-tropospheric layer. The presence of positive composite of MSE exhibit a pronounced gradient as it increases in the south-north direction, culminating with a maximum value over the windward side of the WH (as depicted in Figure 5c). These findings suggest the initiation of convection over the low-lying regions and its intensification over the foothills of the Himalayas. This escalation indicates a high atmospheric instability, subsequently leading to the development of intense convective extreme precipitation. Conversely, the decrease in the MSE seen over the leeward side of the Himalayas indicates that the troposphere is stabilized by cooling and drying processes. In addition, the occurrence of deep convection is dependent on the availability of moisture and the degree of moist convective instability (CI). One method of assessing CI, as defined by (Krishnamurti and Bhalme, 1976; Pattanaik, 2003), involved calculating the difference in moist MSE between 700hPa and 1000hPa. A greater the magnitude of the difference between MSE (at 700hPa) and MSE (at

1000hPa), indicate higher degree of moist convection instability. In the present study, the degree of moist CI is calculated over the WH region during EPEs as illustrated in Figure 5d. A positive anomaly of the CI clearly reveals higher moist convective instability over the foothills of the Himalayas. This moist convective instability, coupled with sufficient moisture availability during the EPEs, amplifies the occurrence of deep convection and, hence, intensify extreme rainfall events.

3.2 Moisture budget and diabatic heating during EPEs

After exploring the dynamic and thermodynamic characteristics, we have now focus on understanding the causes of changes in EPEs during ISM by analysing the moisture budget components based on Equation 5, as proposed by Oueslati et al., (2019). Our analysis provides a physically based quantification of the dynamic and thermodynamic contributions that are useful for EPEs attribution over WH. Figure 6a illustrates all components of the moisture budget and its contribution in percentage during an EPE over the WH. Result highlights that vertical moisture advection is the dominant factor, contributing significantly more than horizontal advection or evaporation to the EPEs. The finding emphasizes that the positive anomaly of vertical advection (goes more than 40 mm day) is the main driver for EPEs, as it prompts the moistening of the troposphere predominantly through vertical moisture transport, sustaining low-level moisture convergence (as shown in Figure 6b). In contrast, horizontal moisture advection, though positive (goes up to 15 mm day), has a smaller impact, it helps minimize the drying of the troposphere by transporting dry air away from rainy regions, which can also aid in increasing precipitation intensity while, changes in evaporation are negligible during the EPEs (Figure 6a, c). The findings underscore the importance of atmospheric circulation, particularly vertical motions, in causing EPEs over WH.

To delve deeper into the mechanisms driving EPEs in these regions, we specifically examine the primary factor: vertical moisture advection. Utilizing equation 6, we decompose vertical moisture advection into dynamic and thermodynamic components. This breakdown allows for the quantification of vertically-integrated changes in dynamic and thermodynamic processes, while accounting for the influence of temperature lapse-rate variations (Goswami et al., 2014; Yanai & Tomita, 1998). Figure 6(d, e) illustrates the contributions, showing that the dynamic term is the primary driver of vertical moisture advection over the study region. It is found that dynamic processes contribute more than 90% to the overall vertical moisture transport. According to equation 4, changes in the vertical pressure velocity (omega) play a crucial role in driving the dynamic contribution. Conversely, alterations in specific humidity are more directly associated with the thermodynamic component. Further manifestations on the spatiotemporal distribution of EPEs, apparent heat source (Q1), moisture sink (Q2), are analyzed to determine the thermodynamic feedback. The monsoon circulation primarily results from large-scale distribution of heat source, which governs convective activity. Thus, the tropical-subtropical deep convection resulted in heavy precipitation is accompanied with the atmospheric diabatic heating which representative of thermodynamic forcing induced by convective activity in the atmosphere (Bhide et al., 1997). Q1 and Q2 are basic measures for analysing the mechanisms of the heating process. The prominent location of Q1 and Q2 align closely with the heavy precipitation centre during the same time over the WH. Q1 denotes the heating generated by convection, radiation, condensation, and eddy heat flux processes, while Q2 is related to the moisture sink resulting from net condensation and divergence in eddy moisture transport. (Han et al., 2021; Son et al., 2021; Xing et al., 2016). Figure. 7 (a, b) show the distribution of vertically integrated heat source Q1 and moisture sink Q2 respectively for EPEs. An intense heat source is observed over the foothills of Himalayas that indicates dominance in convection and radiative heating (Figure 7a). We also noted that the centre of maxima in the spatial distribution of Q2 is also over the same region of WH as Q1 but lesser in magnitude (Figure 7b) indicating that condensation also play significant role to the extreme precipitation. However, the anomalous Q2 extends not as broadly as the Q1, but their centers lie over the same place. A glance at these figures reveals that heating over the foothills of the Himalayas is not only contributed by radiative heating and convection but also by condensation due to latent heating. The vertical distribution of Q1 and Q2 is shown in Figure 7(c, d), respectively in the latitude plain along a WH. The south–north alignment of Q1 and Q2 over the WH is observed. The whole troposphere is occupied by relatively high Q1 in the WH with a peak in the 400hPa–600hPa. Overall, the apparent heating intensity indicates that the mid-troposphere experiences warming during heavy precipitation. The intensified heating in the atmospheric column increases instability in the mid-troposphere and reinforces convective motion. This process involves the upward pumping of warm, moist air from lower levels to higher levels. Furthermore, Figure (7e, f) illustrates the area-averaged vertical profiles of Q1 and Q2 over the WH to elucidate the vertical structure of diabatic heating during EPEs. The findings indicate that the heating maxima are observed in the middle to upper troposphere in the WH, while below 600hPa, the moisture sink exhibits its highest intensity (Figure 7f). In contrast, the heat source appears relatively weaker in the same region (Figure 7e). These results suggest that the latent heat released from the net condensation of water vapor in the lower troposphere does not promptly contribute to atmospheric heating at the corresponding height.

Instead, a substantial amount of latent heat generated at lower levels is rapidly transported upwards by the ascending motion induced by orography, leading to increased convection and the occurrence of extreme precipitation.

3.3 Cloud Microphysical Characteristics

The characteristics of heating profiles are significantly influenced by microphysical processes and its crucial for understanding EPEs in complex regions such as the Himalayas (Baisya et al., 2018; Ganjir et al., 2022; Luo et al., 2009; Rajeevan et al., 2010). Cloud hydrometeors play a pivotal role in shaping precipitation patterns during EPEs, impacting convective dynamics and precipitation intensity (Rogers et al., 2007). The interaction between dynamics, thermodynamics, and cloud microphysics is a key factor in precipitation formation, with microphysical process rates holding significant influence (Chaudhuri et al., 2015; Hazra et al., 2016, 2017). Thus, to fully understand the formation of precipitation leading to EPEs, it is important to consider the accumulation of moisture content coinciding with high vertical velocity, which triggers updrafts and generates deep convective clouds with various microphysical classes such as cloud liquid water, cloud ice water, snow water, supercooled liquid water, and water vapour. This study elucidates to understand the role of the hydrometeor type by linkages between cloud microphysics and large-scale dynamics. Firstly, the spatial distribution of composite anomalies of total column hydrometeors are examined shown in Figure (8a, d). Results clearly show that total column cloud snow water is dominating, followed by total column liquid water specifically over the foothills of Himalayas core precipitation area of the Himalayas. Although total column of cloud ice water (Figure 8b) and supercooled liquid water (Figure 8d) has lesser magnitude than other hydrometeors, but their maximum values concentrated just over foothills of Himalayas, suggesting a sustained contribution during EPEs over WH. Further, vertical-zonal cross-sections of the anomalies of hydrometeors (cloud ice, cloud liquid and, snow water) averaged over the longitude (74°E–82°E) are presented in Figure S3(a-c). Result reveals a highly coherent pattern of cloud ice and cloud snow (as shown in Figure S3(b-c). The finding suggests that snow hydrometeors (Figure S3.c) are the dominant source of rainwater at lower to middle tropospheric levels (800hPa–400hPa). Additionally, there is a noticeable consistency in the distribution of ice hydrometeors (Figure S3b) from middle to upper-pressure levels (500hPa–100hPa). This significant finding indicates that EPEs such as intense cloud bursts over the Himalayan orography region exhibit typical characteristics with large snow water accumulation contributing to liquid and supercooled liquid water. The coherent vertical distribution of cloud snow and ice hydrometeors highlights the importance of snow as a significant component in the formation of rainwater, especially at lower to middle troposphere, while ice hydrometeors play a crucial role in the upper levels of the atmosphere.

3.4 Influence of Extratropical circulation on Himalayan EPEs

We further analyse EPV fields as a potential dynamical precursor of EPEs over the Himalayas. The composite anomaly of isentropic potential vorticity (EPV; on the 330 K surface) displays potential vorticity intrusions indicating the deepening trough and southward advancing cyclonic vorticity stream shown in Figure 9. Upper-level strong cyclonic flows typically accompany positive EPV anomalies, whereas negative EPV anomalies are anticipated to result in high-pressure and anticyclonic flows. The intrusion of positive EPV is associated with strengthening the subtropical jet stream, which can trigger the transport moisture from the AS and the BoB towards the WH. This moisture-laden air encounters the low-pressure system associated with positive EPV, leading to the formation of heavy rainfall. Here, heavy precipitation is generally allied with upper-level EPV intrusions with well-defined features. In addition, Figure 9(b) shows the instruction of EPV two days before the extreme precipitation over the Kedarnath flood 2013, Figure 9(c) during the extreme precipitation day (16-18) June 2013, and Figure 9(d) two day after the extreme precipitation over Kedarnath flood. Result exhibits that due to the entrainment of high EPV air of stratospheric origin, the PV values over the WH are above 4 PV unit associated with tropopause folding during the heavy precipitation days shown in Figure 9(c). Our analysis, however, shows that EPEs during summer impacting the southwest monsoon are linked to positive EPV intrusions and cyclonic patterns of moisture advection. The breaking of Rossby waves, a dominating characteristic contributing to convective severe precipitation, has been linked to incursions of high EPV air from the stratosphere into the tropopause, according to research investigations (Martius et al., 2013; Vellore et al., 2016).

3.5. Role of QRA on the EREs

We further investigate the influence of QRA on the mountain EPEs over the Himalayas. Recent findings (Kornhuber et al., 2017; Mann et al., 2018; Nischal et al., 2024) highlight the significant role of quasi-stationary Rossby waves in shaping weather patterns over the middle-latitude regions across the southern and northern hemispheres. To assess the impact of QRA during EPEs, we adopt the QRA detection scheme proposed by (Kornhuber et al., 2017). Meridional and zonal wind data at 200hPa for extreme events are obtained using ERA5.

Subsequently, these data are subjected to a one-dimensional simple harmonic oscillator analysis. Figures 10(a, b) show the meridional profiles of mean surface temperature for the Kedarnath flood (16-18 June) 2013 and another extreme event in 04-05 September 1995, represented by the red lines, along with their respective climatological averages shown by the blue lines. Finding shows that the temperature gradient decreases to near-zero values around 40̊ N and peaks in the subpolar latitudes. This variation in temperature is associated with QRA, as a rapid warming of the polar regions can affect the jet stream and make it wavier and more prone to QRA. These temperature gradient variations are consistent with the minimum zonal wind and strong westerlies over the mid and polar latitudes shown in Figure 10 (c, d). The double-peaked latitudinal structure in the zonal winds exhibits the expected QRA features. Moreover, Figure 10 (e, f) display the zonal mean of meridional wind at 200hPa, exhibiting a wavy pattern that reflects the high- and low-pressure systems across the poles and tropics, indicating the presence of wave numbers up to eight during both the extreme events. These circumglobally wave patterns show QRA amplification of waves trapped in waveguides and its association of the arctic warming. Results are in lined with recent studies have highlighted the connection between extreme events such as droughts and floods in various parts of the world and the presence of slow-moving amplified Rossby waves, particularly in the midlatitude region of the Northern Hemisphere., QRA (Kornhuber et al., 2017; Lakshmi Kumar et al., 2021; Mann et al., 2018) particular the midlatitude region of Northern Hemisphere. In addition, the zonal wavenumber spectra for the zonally averaged meridional wind from 27°N to 60°N latitudes reveal the peak amplitude at wave numbers five and eight, which are higher than those for the climatological period, as shown in Figure 10 (g, h). These waves can break and cause the transport of moist air from the tropics to the subtropic, and the transport of dry air from the stratosphere to the troposphere. This can create favourable conditions for EREs over the Himalayas, as the moist air can condense and release latent heat, which can enhance atmospheric instability. Based on these results, a schematic representation by connecting important mechanisms responsible for EPEs over the Himalayas is presented in Figure 11.

4. Summary and Conclusion

The Himalayas are a region that is highly vulnerable to the impacts of climate change, including changes in summer precipitation patterns resulting extreme events. Our study is pivotal in unravelling the intricate dynamical, thermodynamical, processes associated with EPEs occurrence over the WH. In summary, studies have shown that the occurrence of EPEs over the WH is linked to large-scale drivers along with localise factors. The following are the main findings from the analysis.

- The findings indicate that the synoptic features and the mesoscale orography forcing contribute significantly to EPEs in the WH. The study proves that favourable synoptic scale conditions, such as low OLR anomaly, high precipitable water, high soil moisture, and surface cooling processes over the WH region, leads to cloud formation and heavy precipitation. Foothills of Himalayan creates the base of steep mountains that influence moisture transport and produce strong gradients for deep convection that leads in EPEs over the Himalayas.
- Study reveals that EPEs occurring over the WH are linked to large-scale circulation patterns that prevail during these EPEs' evolution. This pattern consists of the formation of zonal waves at mid-latitudes and the equatorward movement of westerly troughs. In Addition, low-level wind composites indicate that moisture-laden monsoonal winds from the AS and BoB intensify during EPEs, which is further strengthened by the development of a divergence (cyclonic and anticyclonic gyre) feature in the upper troposphere over the WH. The study result suggests that the interaction between the monsoon circulation and a penetrating mid-latitude westerly trough increases the likelihood of EPEs over WH.
- The results reveal strong MSE build-up in the middle tropospheric over the foothills of Himalayas give the signal initiation of convective activity resulting intense precipitation over WH. In addition, greater degree of moist convective instability, couple with available high moisture during the ISM, can increase the occurrence of deep convection and hence make favourable condition for EPEs.
- Our study comprehensively shown that EPEs over WH are primarily dynamically driven by the induction of stronger vertical motions. This process leads to an increase in the moisture content of the atmospheric column, consequently reinforcing convection. Overall, it has been demonstrated that the dynamic contribution (more than 90 percent) surpasses the contribution from thermodynamic for EPEs. Additionally, diabatic heat forcing showed a maximum in the mid-tropospheric region, indicating the presence of a dominant heat source Q1 and a positive anomaly of apparent moisture sink (Q2) indicated increased moisture sinking at the low-level maximum over the WH.
- Cloud microphysics plays a significant role in modulating the precipitation over such complex terrain regions in the Himalayas. As the wind ascending over the mountains,

it cools and condenses, forming different types of Hydrometeors in clouds. The finding shows that total column cloud snow and liquid water is dominating, followed by total column liquid water, specifically over the WH leading to the formation of large and heavy raindrops that contribute intensification of precipitation.

- The tropical–extratropical interaction involving the intrusion of positive Ertel PV fields provides valuable information for understanding the potential dynamical precursor of EPEs over the Himalayas. The extratropical cyclonic EPV intrusion has been observed over the WH that started deepening southward during the EPEs and provided the external force to enhance the low-level moisture-laden monsoonal wind toward the Himalayas.
- The findings of this study provide compelling evidence supporting the role of QRA as an amplifying mechanism for planetary Rossby waves in the Northern Hemisphere, contributing to the persistence of extreme rainfall episodes over the Himalayas. The distinct imprint of QRA is evident in the atmospheric circulation patterns, notably the double jet zonally averaged zonal wind and the presence of circumglobally meridional wave patterns, both associated with Arctic warming. The observed wavenumber spectra emphasize the significance of waves at higher numbers, primarily five and eight, during EPEs. These results elucidate the intricate dynamics linking QRA, Arctic warming, and the manifestation of specific atmospheric patterns, providing valuable insights into the mechanisms influencing prolonged and intense precipitation events over the Himalayan region insights into the linkages between large-scale atmospheric phenomena and localized extreme weather occurrences.

In conclusion, this comprehensive study sheds light on the cause behind in escalating EPEs over the WH. By delving into synoptic, mesoscale, and large-scale factors, our findings underscore the intricate dynamics governing EPEs in this vulnerable region. The identified links between large-scale circulation patterns, orographic features, and microphysical processes provide crucial insights for understanding and predicting intensified precipitation. This research not only advances our comprehension of Himalayan climate dynamics but also underscores the pressing need for continued investigation into the nuanced interactions shaping extreme weather events in this critical geographical expanse.

Acknowledgements:

Authors gratefully acknowledge the IISER Mohali for providing the essential facilities and resources that facilitated the successful completion of this research. Rohtash gratefully acknowledges the financial assistance as a Senior Research Fellow from the Prime Minister's Research Fellowship (PMRF), Ministry of Education, Government of India. The authors are thankful to the Ministry of Earth Sciences (MoES/16/03/2021-RDESS/NARM-3), Government of India for funding this research.

Author Statement

Rohtash Saini: Writing-Original draft preparation, Methodology, Software, Formal Analysis, Visualization. **Raju Attada**: Conceptualization, Formal Analysis, Supervision, Resources, Writing-review and editing.

References:

Aggarwal, D., Attada, R., Shukla, K. K., Chakraborty, R., & Kunchala, R. K. (2021). Monsoon precipitation characteristics and extreme precipitation events over Northwest India using Indian high resolution regional reanalysis. *Atmospheric Research*, *267*(August 2021), 105993. https://doi.org/10.1016/j.atmosres.2021.105993

Ahmad, M., Kumari, M., Kumar, N., Goswami, G., Shahfahad, & Asgher, M. S. (2023). Assessing livelihood vulnerability to climate variability in the Himalayan region: a district-level analysis of Jammu Province, India. *GeoJournal*, (0123456789). https://doi.org/10.1007/s10708-023-10829-2

Allen, M. R., & Ingram, W. J. (2002). Constraints on future changes in climate and the hydrologic cycle. *Nature*, *419*(6903). https://doi.org/10.1038/nature01092

Andersen, J. A., & Kuang, Z. (2012). Moist static energy budget of MJO-like disturbances in the atmosphere of a zonally symmetric aquaplanet. *Journal of Climate*, *25*(8), 2782–2804. https://doi.org/10.1175/JCLI-D-11-00168.1

Attada, R., Dasari, H. P., Kunchala, R. K., Langodan, S., Kumar, K. N., Knio, O., & Hoteit, I. (2020). Evaluating cumulus parameterization schemes for the simulation of Arabian Peninsula winter rainfall. *Journal of Hydrometeorology*, *21*(5), 1089–1114. https://doi.org/10.1175/JHM-D-19-0114.1

Baisya, H., Pattnaik, S., Hazra, V., Sisodiya, A., & Rai, D. (2018). Ramifications of Atmospheric Humidity on Monsoon Depressions over the Indian Subcontinent. *Scientific Reports*, *8*(1), 1–9. https://doi.org/10.1038/s41598-018-28365-2

Bhardwaj, A., Wasson, R. J., Ziegler, A. D., Chow, W. T. L., & Sundriyal, Y. P. (2019). Characteristics of rain-induced landslides in the Indian Himalaya: A case study of the Mandakini Catchment during the 2013 flood. *Geomorphology*, *330,* 100–115. https://doi.org/10.1016/j.geomorph.2019.01.010

Bharti, V. (2015). Investigation of Extreme Rainfall Events Over the Northwest Himalaya Region Using Satellite Dat (Master's thesis, University of Twente).

Bharti, V., Singh, C., Ettema, J., & Turkington, T. A. R. (2016). Spatiotemporal characteristics of extreme rainfall events over the Northwest Himalaya using satellite data. *International Journal of Climatology*, *36*(12), 3949–3962. https://doi.org/10.1002/joc.4605

Bhide, U. V., Mujamdar, V. R., Ghanekar, S. P., Paul, D. K., Chen, T.-C., & Rao, G. V. (1997). A diagnostic study on heat sources and moisture sinks in the monsoon trough area during active-break phases of the Indian summer monsoon, 1979. *Tellus A: Dynamic Meteorology and Oceanography*, *49*(4), 455. https://doi.org/10.3402/tellusa.v49i4.14683

Bohlinger, P., Sorteberg, A., & Sodemann, H. (2017). Synoptic conditions and moisture sources actuating extreme precipitation in Nepal. *Journal of Geophysical Research: Atmospheres*, *122*(23), 12,653-12,671. https://doi.org/10.1002/2017JD027543

Byrne, M. P., & Schneider, T. (2016). Narrowing of the ITCZ in a warming climate: Physical mechanisms. *Geophysical Research Letters*, *43*(21), 11,350-11,357. https://doi.org/10.1002/2016GL070396

Ccoica-López, K. L., Pasapera-Gonzales, J. J., & Jimenez, J. C. (2019). Spatio-temporal variability of the precipitable water vapor over peru through MODIS and ERA-interim time series. *Atmosphere*, *10*(4). https://doi.org/10.3390/ATMOS10040192

Chansaengkrachang, K., Luadsong, A., & Aschariyaphotha, N. (2018). Vertically integrated moisture flux convergence over southeast Asia and its relation to rainfall over Thailand. *Pertanika Journal of Science and Technology*, *26*(1), 235–246.

Chaudhuri, C., Tripathi, S., Srivastava, R., & Misra, A. (2015). Observation- and numerical-analysis-based dynamics of the Uttarkashi cloudburst. *Annales Geophysicae*, *33*(6), 671–686. https://doi.org/10.5194/angeo-33-671-2015

Chevuturi, A., & Dimri, A. P. (2016). Investigation of Uttarakhand (India) disaster-2013 using weather research and forecasting model. *Natural Hazards*, *82*(3), 1703–1726. https://doi.org/10.1007/s11069-016-2264-6

Dahri, Z. H., Ludwig, F., Moors, E., Ahmad, B., Khan, A., & Kabat, P. (2016). An appraisal of precipitation distribution in the high-altitude catchments of the Indus basin. *Science of the Total Environment*, *548–549*, 289–306. https://doi.org/10.1016/j.scitotenv.2016.01.001

Das, L., & Meher, J. K. (2019). Drivers of climate over the Western Himalayan region of India: A review. *Earth-Science Reviews*, *198*, 102935. https://doi.org/10.1016/j.earscirev.2019.102935

Das, S., Ashrit, R., & Moncrieff, M. W. (2006). Simulation of a Himalayan cloudburst event. *Journal of Earth System Science*, *115*(3), 299–313. https://doi.org/10.1007/BF02702044

Dimri, A. P., Thayyen, R. J., Kibler, K., Stanton, A., Jain, S. K., Tullos, D., & Singh, V. P. (2016). A review of atmospheric and land surface processes with emphasis on flood generation in the Southern Himalayan rivers. *Science of the Total Environment*, *556*, 98–115. https://doi.org/10.1016/j.scitotenv.2016.02.206

Dube, A., Ashrit, R., Ashish, A., Sharma, K., Iyengar, G. R., Rajagopal, E. N., & Basu, S. (2014). Forecasting the heavy rainfall during Himalayan flooding-June 2013. *Weather and Climate Extremes*, 22–34. https://doi.org/10.1016/j.wace.2014.03.004

Fasullo, J., & Webster, P. J. (2003). A hydrological definition of Indian Monsoon onset and withdrawal. *Journal of Climate*, *16*(19), 3200–3211. https://doi.org/10.1175/1520-0442(2003)016<3200a:AHDOIM>2.0.CO;2

Ganjir, G., Pattnaik, S., & Trivedi, D. (2022). Characteristics of dynamical and thermo-dynamical variables during heavy rainfall events over the Indian region. *Dynamics of Atmospheres and Oceans*, *99*(February), 101315. https://doi.org/10.1016/j.dynatmoce.2022.101315

George, B., & Kutty, G. (2021). Ensemble sensitivity analysis of an extreme rainfall event over the Himalayas in June 2013. *Dynamics of Atmospheres and Oceans*, *93*, 101202. https://doi.org/10.1016/J.DYNATMOCE.2021.101202

Goswami, B. B., Deshpande, M., Mukhopadhyay, P., Saha, S. K., Rao, S. A., Murthugudde, R., & Goswami, B. N. (2014). Simulation of monsoon intraseasonal variability in NCEP CFSv2 and its role on systematic bias. *Climate Dynamics*, *43*(9–10), 2725–2745. https://doi.org/10.1007/s00382-014-2089-5

Han, Y., Ma, W., Yang, Y., Ma, Y., Xie, Z., Sun, G., et al. (2021). Impacts of the Silk Road pattern on the interdecadal variations of the atmospheric heat source over the Tibetan Plateau. *Atmospheric Research*, *260*(October 2020), 105696. https://doi.org/10.1016/j.atmosres.2021.105696

Hazra, A., Chaudhari, H. S., & Dhakate, A. (2016). Evaluation of cloud properties in the

NCEP CFSv2 model and its linkage with Indian summer monsoon. *Theoretical and Applied Climatology*, *124*(1–2), 31–41. https://doi.org/10.1007/s00704-015-1404-3

Hazra, A., Chaudhari, H. S., Ranalkar, M., & Chen, J. P. (2017). Role of interactions between cloud microphysics, dynamics and aerosol in the heavy rainfall event of June 2013 over Uttarakhand, India. *Quarterly Journal of the Royal Meteorological Society*, *143*(703), 986–998. https://doi.org/10.1002/qj.2983

Hegdahl, T. J., Tallaksen, L. M., Engeland, K., Burkhart, J. F., & Xu, C. Y. (2016). Discharge sensitivity to snowmelt parameterization: A case study for Upper Beas basin in Himachal Pradesh, India. *Hydrology Research*, *47*(4), 683–700. https://doi.org/10.2166/nh.2016.047

Hersbach, H., & Dee, D. (2016). ERA5 reanalysis is in production, ECMWF Newsletter 147, ECMWF. *ECMWF Newsletter*, *147*(Spring 2016), 7.

Houze, R. A. (2014). Mesoscale convective systems. *International Geophysics*, *104*, 237–286. https://doi.org/10.1016/B978-0-12-374266-7.00009-3

Houze, R. A., McMurdie, L. A., Rasmussen, K. L., Kumar, A., & Chaplin, M. M. (2017). Multiscale Aspects of the Storm Producing the June 2013 Flooding in Uttarakhand, India. *Monthly Weather Review*, *145*(11), 4447–4466. https://doi.org/10.1175/MWR-D-17-0004.1

Hunt, K. M. R., & Parker, D. J. (2016). The movement of Indian monsoon depressions by interaction with image vortices near the Himalayan wall. *Quarterly Journal of the Royal Meteorological Society*, *142*(698), 2224–2229. https://doi.org/10.1002/qj.2812

Hunt, K. M. R., Turner, A. G., & Shaffrey, L. C. (2018a). Extreme daily rainfall in Pakistan and North India: Scale interactions, mechanisms, and precursors. *Monthly Weather Review*, *146*(4), 1005–1022. https://doi.org/10.1175/MWR-D-17-0258.1

Hunt, K. M. R., Turner, A. G., & Shaffrey, L. C. (2018b). The evolution, seasonality and impacts of western disturbances. *Quarterly Journal of the Royal Meteorological Society*, *144*(710), 278–290. https://doi.org/10.1002/qj.3200

Immerzeel, W. W., Droogers, P., de Jong, S. M., & Bierkens, M. F. P. (2009). Large-scale monitoring of snow cover and runoff simulation in Himalayan river basins using remote sensing. *Remote Sensing of Environment*, *113*(1), 40–49. https://doi.org/10.1016/j.rse.2008.08.010

Jain, S., Jain, S., Jain, N., & Xu, C.-Y. (2017). Hydrologic modeling of a Himalayan mountain basin by using the SWAT mode. *Hydrology and Earth System Sciences Discussions*, (March), 1–26. https://doi.org/10.5194/hess-2017-100

Jiang, X., Yuan, H., Xue, M., Chen, X., & Tan, X. (2014). Analysis of a heavy rainfall event over Beijing during 21-22 july 2012 based on high resolution model analyses and forecasts. *Journal of Meteorological Research*, *28*(2), 199–212. https://doi.org/10.1007/s13351-014-3139-y

Johnson, D. R. (1987). Global and regional distributions fo atmospheric heat sources and sinks during the GWE. *Monsoon Meteorology*, pp.271-297

Joseph, S., Sahai, A. K., Sharmila, S., Abhilash, S., Borah, N., Chattopadhyay, R., et al. (2015). North Indian heavy rainfall event during June 2013: diagnostics and extended range prediction. *Climate Dynamics*, *44*(7–8), 2049–2065. https://doi.org/10.1007/s00382-014-2291-5

Kad, P., & Ha, K.-J. (2023). Recent tangible interannual variability of monsoonal orographic rainfall in the Eastern Himalayas. *Authorea Preprints*. https://doi.org/10.1029/2023JD038759

Kadel, I., Yamazaki, T., Iwasaki, T., & Abdillah, M. R. (2018). Projection of future monsoon precipitation over the central himalayas by CMIP5 models under warming scenarios. *Climate Research*, *75*(1), 1–21. https://doi.org/10.3354/cr01497

Karki, R., Hasson, S. ul, Gerlitz, L., Talchabhadel, R., Schenk, E., Schickhoff, U., et al. (2018a). WRF-based simulation of an extreme precipitation event over the Central Himalayas: Atmospheric mechanisms and their representation by microphysics parameterization schemes. *Atmospheric Research*, *214*, 21–35. https://doi.org/10.1016/j.atmosres.2018.07.016

Karki, R., Hasson, S. ul, Gerlitz, L., Talchabhadel, R., Schenk, E., Schickhoff, U., et al. (2018b). WRF-based simulation of an extreme precipitation event over the Central Himalayas: Atmospheric mechanisms and their representation by microphysics parameterization schemes. *Atmospheric Research*, *214*(February), 21–35. https://doi.org/10.1016/j.atmosres.2018.07.016

Kornhuber, K., Petoukhov, V., Karoly, D., Petri, S., Rahmstorf, S., & Coumou, D. (2017). Summertime planetary wave resonance in the Northern and Southern hemispheres. *Journal of Climate*, *30*(16), 6133–6150. https://doi.org/10.1175/JCLI-D-16-0703.1

Kotal, S. D., Roy, S. Sen, & Roy Bhowmik, S. K. (2014). Catastrophic heavy rainfall episode over Uttarakhand during 16-18 June 2013 - observational aspects. *Current Science*, *107*(2), 234–245.

Krishnamurti, T. N., & Bhalme, H. N. (1976). Oscillations of a Monsoon System. Part I. Observational Aspects. *Journal of the Atmospheric Sciences*, *33*(10), 1937–1954.

https://doi.org/10.1175/1520-0469(1976)033<1937:OOAMSP>2.0.CO;2

Krishnan, R., Sabin, T. P., Madhura, R. K., Vellore, R. K., Mujumdar, M., Sanjay, J., et al. (2019). Non-monsoonal precipitation response over the Western Himalayas to climate change. *Climate Dynamics*, *52*(7–8), 4091–4109. https://doi.org/10.1007/s00382-018-4357-2

Kumar, A., Houze, R. A., Rasmussen, K. L., & Peters-Lidard, C. (2014). Simulation of a flash flooding storm at the steep edge of the Himalayas. *Journal of Hydrometeorology*, *15*(1), 212–228. https://doi.org/10.1175/JHM-D-12-0155.1

Kunkel, K. E., Karl, T. R., Squires, M. F., Yin, X., Stegall, S. T., & Easterling, D. R. (2020). Precipitation extremes: Trends and relationships with average precipitation and precipitable water in the contiguous United States. *Journal of Applied Meteorology and Climatology*, *59*(1), 125–142. https://doi.org/10.1175/JAMC-D-19-0185.1

Lakshmi Kumar, T. V., Durga, G. P., Rao, K. K., Barbosa, H., Kulkarni, A., Patwardhan, S., et al. (2021). Connection of Quasi-Resonant Amplification to the Delay in Atmospheric Residence Times Over India. *Frontiers in Earth Science*, *9*(April), 1–10. https://doi.org/10.3389/feart.2021.615325

Li, H., Xu, C. Y., Beldring, S., Tallaksen, L. M., & Jain, S. K. (2016). Water resources under climate change in himalayan basins. *Water Resources Management*, *30*(2), 843–859. https://doi.org/10.1007/s11269-015-1194-5

Luo, Y., Zhang, R., & Wang, H. (2009). Comparing occurrences and vertical structures of hydrometeors between eastern China and the Indian monsoon region using cloudsat/CALIPSO data. *Journal of Climate*, *22*(4), 1052–1064. https://doi.org/10.1175/2008JCLI2606.1

Malik, N., Bookhagen, B., & Mucha, P. J. (2016). Spatiotemporal patterns and trends of Indian monsoonal rainfall extremes. *Geophysical Research Letters*, *43*(4), 1710–1717. https://doi.org/10.1002/2016GL067841

Maloney, E. D. (2009). The moist static energy budget of a composite tropical intraseasonal oscillation in a climate model. *Journal of Climate*, *22*(3), 711–729. https://doi.org/10.1175/2008JCLI2542.1

Mann, M. E., Rahmstorf, S., Kornhuber, K., Steinman, B. A., Miller, S. K., Petri, S., & Coumou, D. (2018). Projected changes in persistent extreme summer weather events: The role of quasi-resonant amplification. *Science Advances*, *4*(10), 1–10. https://doi.org/10.1126/sciadv.aat3272

Martius, O., Sodemann, H., Joos, H., Pfahl, S., Winschall, A., Croci-Maspoli, M., et al.

(2013). The role of upper-level dynamics and surface processes for the pakistan flood of July 2010. *Quarterly Journal of the Royal Meteorological Society*, *139*(676), 1780–1797. https://doi.org/10.1002/qj.2082

Medina, S., Houze, R. A., Kumar, A., & Niyogi, D. (2010). Summer monsoon convection in the Himalayan region: Terrain and land cover effects. *Quarterly Journal of the Royal Meteorological Society*, *136*(648), 593–616. https://doi.org/10.1002/qj.601

Mukhopadhyay, P., Taraphdar, S., Goswami, B. N., & Krishnakumar, K. (2010). Indian summer monsoon precipitation climatology in a high-resolution regional climate model: Impacts of convective parameterization on systematic biases. *Weather and Forecasting*, *25*(2), 369–387. https://doi.org/10.1175/2009WAF2222320.1

Nandargi, S., & Dhar, O. N. (2011). Extreme rainfall events over the Himalayas between 1871 and 2007. *Hydrological Sciences Journal*, *56*(6), 930–945. https://doi.org/10.1080/02626667.2011.595373

Narasimha Rao, N., Paul, S., Skekhar, M. S., Singh, G. P., Mitra, A. K., & Bhan, S. C. (2021). Unprecedented heavy rainfall event over Yamunanagar, India during 14 July 2016: An observational and modelling study. *Meteorological Applications*, *28*(6), 1–15. https://doi.org/10.1002/met.2039

Negi, V. S., Thakur, S., Dhyani, R., Bhatt, I. D., & Rawal, R. S. (2021). Climate change observations of indigenous communities in the Indian Himalaya. *Weather, Climate, and Society*, *13*(2), 245–257. https://doi.org/10.1175/WCAS-D-20-0077.1

Nischal, Rohtash, K, S., Pathaikara, A., Punde, P., & Attada, R. (2023). Hydrological Extremes in Western Himalayas-Trends and Their Physical Factors. In *Natural Hazards - New Insights [Working Title]*. IntechOpen. https://doi.org/10.5772/intechopen.109445

Nischal, Attada, R., Hunt, K. M. R., & Barlow, M. (2024). Underlying physical mechanisms of winter precipitation extremes over India's high mountain region. *Quarterly Journal of the Royal Meteorological Society*, (December 2023), 1–23. https://doi.org/10.1002/qj.4661

Oueslati, B., Yiou, P., & Jézéquel, A. (2019). Revisiting the dynamic and thermodynamic processes driving the record-breaking January 2014 precipitation in the southern UK. *Scientific Reports*, *9*(1), 1–7. https://doi.org/10.1038/s41598-019-39306-y

Pall, P., Allen, M. R., & Stone, D. A. (2007). Testing the Clausius-Clapeyron constraint on changes in extreme precipitation under CO2 warming. *Climate Dynamics*, *28*(4), 351–363. https://doi.org/10.1007/s00382-006-0180-2

Pattanaik, D. R. (2003). Analysis of moist convective instability over Indian monsoon region

and neighbourhood. *Mausam*, *54*(3), 659–670. https://doi.org/10.54302/mausam.v54i3.1557
Paula Barros, A., & Lettenmaier, P. (1994). Dynamic Modeling of Orographically Induced Precipitation, *32*(94), 265–284.
Pepin, N., Bradley, R. S., Diaz, H. F., Baraer, M., Caceres, E. B., Forsythe, N., et al. (2015). Elevation-dependent warming in mountain regions of the world. *Nature Climate Change*, *5*(5), 424–430. https://doi.org/10.1038/nclimate2563
Pfahl, S., O'Gorman, P. A., & Fischer, E. M. (2017). Understanding the regional pattern of projected future changes in extreme precipitation. *Nature Climate Change*, *7*(6), 423–427. https://doi.org/10.1038/nclimate3287
Priya, P., Krishnan, R., Mujumdar, M., & Houze, R. A. (2017). Changing monsoon and midlatitude circulation interactions over the Western Himalayas and possible links to occurrences of extreme precipitation. *Climate Dynamics*, *49*(7–8), 2351–2364. https://doi.org/10.1007/s00382-016-3458-z
Rajeevan, M., Kesarkar, A., Thampi, S. B., Rao, T. N., Radhakrishna, B., & Rajasekhar, M. (2010). Sensitivity of WRF cloud microphysics to simulations of a severe thunderstorm event over Southeast India. *Annales Geophysicae*, *28*(2), 603–619. https://doi.org/10.5194/angeo-28-603-2010
Raju, A., Parekh, A., Chowdary, J. S., & Gnanaseelan, C. (2015). Assessment of the Indian summer monsoon in the WRF regional climate model. *Climate Dynamics*, *44*(11–12), 3077–3100. https://doi.org/10.1007/s00382-014-2295-1
Ranalkar, M. R., Chaudhari, H. S., Hazra, A., Sawaisarje, G. K., & Pokhrel, S. (2016). Dynamical features of incessant heavy rainfall event of June 2013 over Uttarakhand, India. *Natural Hazards*, *80*(3), 1579–1601. https://doi.org/10.1007/s11069-015-2040-z
Rasmussen, K. L., & Houze, R. A. (2012). A flash-flooding storm at the steep edge of high terrain. *Bulletin of the American Meteorological Society*, *93*(11), 1713–1724. https://doi.org/10.1175/BAMS-D-11-00236.1
Rogers, R. F., Black, M. L., Chen, S. S., & Black, R. A. (2007). An evaluation of microphysics fields from mesoscale model simulations of tropical cyclones. Part I: Comparisons with observations. *Journal of the Atmospheric Sciences*, *64*(6), 1811–1834. https://doi.org/10.1175/JAS3932.1
Roy, S., Bose, A., & Chowdhury, I. R. (2021). Flood risk assessment using geospatial data and multi-criteria decision approach: a study from historically active flood-prone region of Himalayan foothill, India. *Arabian Journal of Geosciences*, *14*(11).

https://doi.org/10.1007/s12517-021-07324-8

Sabin, T. P., Krishnan, R., Vellore, R., Priya, P., Borgaonkar, H. P., Singh, B. B., & Sagar, A. (2020). Climate Change Over the Himalayas. In *Assessment of Climate Change over the Indian Region* (pp. 207–222). Singapore: Springer Singapore. https://doi.org/10.1007/978-981-15-4327-2_11

Sain, K., Mehta, M., & Kumar, V. (2022). Heavy Rainfall-triggered Flash Floods around the Amarnath Holy Cave. *Journal of the Geological Society of India*, *98*(9), 1323–1324. https://doi.org/10.1007/s12594-022-2170-3

Saini, R., & Attada, R. (2023). Analysis of Himalayan summer monsoon rainfall characteristics using Indian High-Resolution Regional Reanalysis. *International Journal of Climatology*, (April), 1–22. https://doi.org/10.1002/joc.8087

Saini, R., Sharma, N., & Attada, R. (2023). Delving into Recent Changes in Precipitation Patterns in the Western Himalayas under Global Warming. *Global Warming - A Concerning Component of Climate Change*. https://doi.org/10.5772/intechopen.1002028

Sandhya, M., Sridharan, S., & Indira Devi, M. (2015). Tropical upper tropospheric humidity variations due to potential vorticity intrusions. *Annales Geophysicae*, *33*(9), 1081–1089. https://doi.org/10.5194/angeo-33-1081-2015

Schomburg, A., Venema, V., Ament, F., & Simmer, C. (2012). Application of an adaptive radiative transfer scheme in a mesoscale numerical weather prediction model. *Quarterly Journal of the Royal Meteorological Society*, *138*(662), 91–102. https://doi.org/10.1002/qj.890

Shekhar, M. S., Devi, U., Paul, S., Singh, G. P., & Singh, A. (2017). Analysis of trends in extreme precipitation events over Western Himalaya Region: intensity and duration wise study. *Journal of Indian Geophysical Union*, *21*(3), 223–229.

Shen, X., Wu, X., Xie, X., Ma, Z., & Yang, M. (2017). Spatiotemporal Analysis of Drought Characteristics in Song-Liao River Basin in China. *Advances in Meteorology*, *2017*. https://doi.org/10.1155/2017/3484363

Shrestha, P., Dimri, A. P., Schomburg, A., & Simmer, C. (2015). Improved understanding of an extreme rainfall event at the Himalayan foothills - a case study using COSMO. *Tellus, Series A: Dynamic Meteorology and Oceanography*, *67*(1), 1–13. https://doi.org/10.3402/tellusa.v67.26031

Singh, D., Sharma, V., & Juyal, V. (2015). Observed linear trend in few surface weather elements over the northwest Himalayas (NWH) during winter season. *Journal of Earth System Science*, *124*(3), 553–565. https://doi.org/10.1007/s12040-015-0560-2

Singh, R., Siingh, D., Gokani, S. A., Sreeush, M. G., Buchunde, P. S., Maurya, A. K., et al. (2015). Brief Communication: Climatic, meteorological and topographical causes of the 16-17 June 2013 Kedarnath (India) natural disaster event. *Natural Hazards and Earth System Sciences*, *15*(7), 1597–1601. https://doi.org/10.5194/nhess-15-1597-2015

Singh, S., & Lal Kansal, M. (2022). Cloudburst Induced Flood Assessment in the North-Western Himalayan Region—A Case Study of Upper Beas Basin. *5th World Congress on Disaster Management*, 89–99. https://doi.org/10.4324/9781003341932-11

Son, J. H., Seo, K. H., Son, S. W., & Cha, D. H. (2021). How Does Indian Monsoon Regulate the Northern Hemisphere Stationary Wave Pattern? *Frontiers in Earth Science*, *8*(January), 1–10. https://doi.org/10.3389/feart.2020.599745

Sravana Kumar, M., Shekhar, M. S., Rama Krishna, S. S. V. S., Bhutiyani, M. R., & Ganju, A. (2012). Numerical simulation of cloud burst event on August 05, 2010, over Leh using WRF mesoscale model. *Natural Hazards*, *62*(3), 1261–1271. https://doi.org/10.1007/s11069-012-0145-1

Sudharsan, N., Karmakar, S., Fowler, H. J., & Hari, V. (2020). Large-scale dynamics have greater role than thermodynamics in driving precipitation extremes over India. *Climate Dynamics*, *55*(9–10), 2603–2614. https://doi.org/10.1007/s00382-020-05410-3

Trenberth, K.E., Houghton, J.T. & Filho, L. G. . (1995). The Science of Climate. *The Climate System, In: Climate Change*.

Trenberth, K. E., & Guillemot, C. J. (1998). Evaluation of the atmospheric moisture and hydrological cycle in the NCEP/NCAR reanalyses. *Climate Dynamics*, *14*(3), 213–231. https://doi.org/10.1007/s003820050219

Ullah, K., & Shouting, G. (2013). A diagnostic study of convective environment leading to heavy rainfall during the summer monsoon 2010 over Pakistan. *Atmospheric Research*, *120–121*, 226–239. https://doi.org/10.1016/j.atmosres.2012.08.021

Vellore, R. K., Kaplan, M. L., Krishnan, R., Lewis, J. M., Sabade, S., Deshpande, N., et al. (2016). Monsoon-extratropical circulation interactions in Himalayan extreme rainfall. *Climate Dynamics*, *46*(11–12), 3517–3546. https://doi.org/10.1007/s00382-015-2784-x

Vellore, R. K., Bisht, J. S., Krishnan, R., Uppara, U., Di Capua, G., & Coumou, D. (2020). *Sub-synoptic circulation variability in the Himalayan extreme precipitation event during June 2013*. *Meteorology and Atmospheric Physics* (Vol. 132). Springer Vienna. https://doi.org/10.1007/s00703-019-00713-5

Wang, B., Bao, Q., Hoskins, B., Wu, G., & Liu, Y. (2008). Tibetan Plateau warming and precipitation changes in East Asia. *Geophysical Research Letters*, *35*(14), 1–5.

https://doi.org/10.1029/2008GL034330

Wang, F., Shao, W., Yu, H., Kan, G., He, X., Zhang, D., et al. (2020). Re-evaluation of the Power of the Mann-Kendall Test for Detecting Monotonic Trends in Hydrometeorological Time Series. *Frontiers in Earth Science, 8*(February), 1–12. https://doi.org/10.3389/feart.2020.00014

Xing, N., Li, J., & Wang, L. (2016). Effect of the early and late onset of summer monsoon over the Bay of Bengal on Asian precipitation in May. *Climate Dynamics*, *47*(5–6), 1961–1970. https://doi.org/10.1007/s00382-015-2944-z

Yanai, M., & Tomita, T. (1998). Seasonal and interannual variability of atmospheric heat sources and moisture sinks as determined from NCEP-NCAR reanalysis. *Journal of Climate*, *11*(3), 463–482. https://doi.org/10.1175/1520-0442(1998)011<0463:SAIVOA>2.0.CO;2

Zhang, H., Henderson-Sellers, A., & Mcguffie, K. (2001). The compounding effects of tropical deforestation and greenhouse warming on climate. *Climatic Change*, *49*(3), 309–338. https://doi.org/10.1023/A:1010662425950

Zheng, T., Feng, T., Xu, K., & Cheng, X. (2020). Precipitation and the Associated Moist Static Energy Budget off Western Australia in Conjunction with Ningaloo Niño. *Frontiers in Earth Science, 8*(November), 1–13. https://doi.org/10.3389/feart.2020.597915

List of Figures

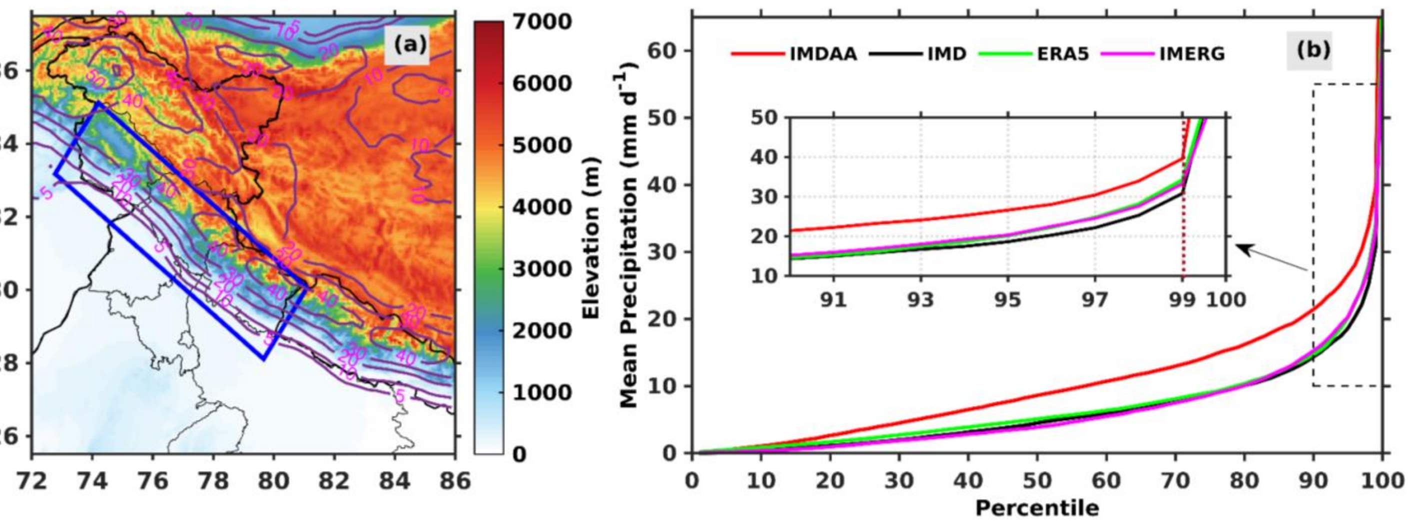

Figure1: (a) Topography (shaded units in meters) map of Indian Himalayas with blue rectangle indicating Himalayan foothills region. Magenta counters represent the topography complexity (%) derived from GTOP030 data, and (b) Mean precipitation (mm day^{-1}) versus percentile over Himalayan foothills.

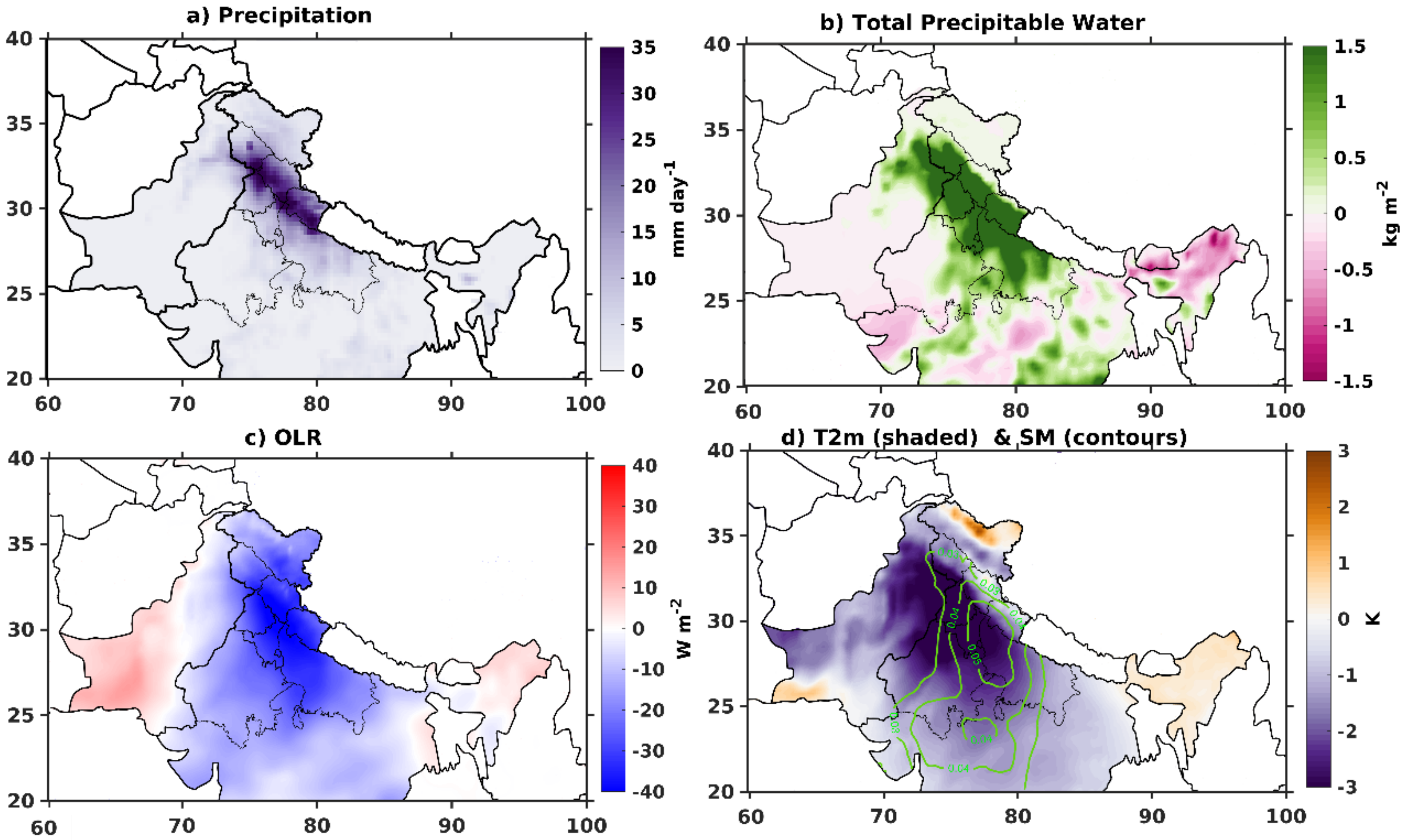

Figure 2: Composite anomalies of (a) precipitation, (b) total precipitable water, (c) outgoing longwave radiation (OLR), (d) 2-meter air temperature and green color contours represents the soil moisture during ISM extreme precipitation events occurring over the Himalaya during 1979-2020.

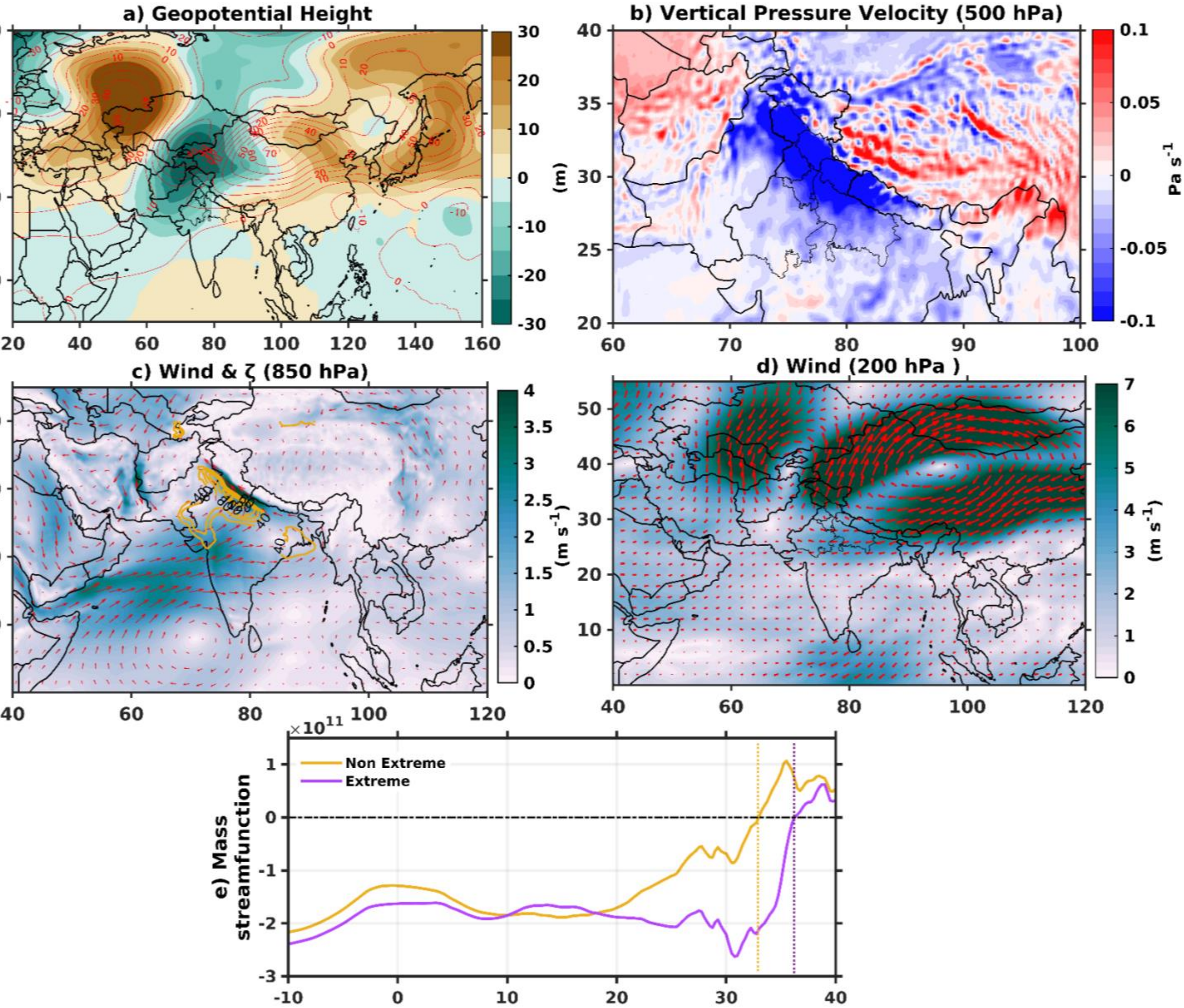

Figure 3: Composite anomalies of (a) geopotential height at 200hPa (contours) and 500hPa (shaded), (b) mid-tropospheric vertical pressure velocity (c) wind at 850hPa (vectors), and the relative vorticity (counters), (d) tropospheric wind at 200hPa for summer monsoon extreme precipitation events, and (e) represents the mass stream function (kg sec^{-1}) during extreme days and non-extreme days (shown in yellow line) over the Himalayas during 1979-2020.

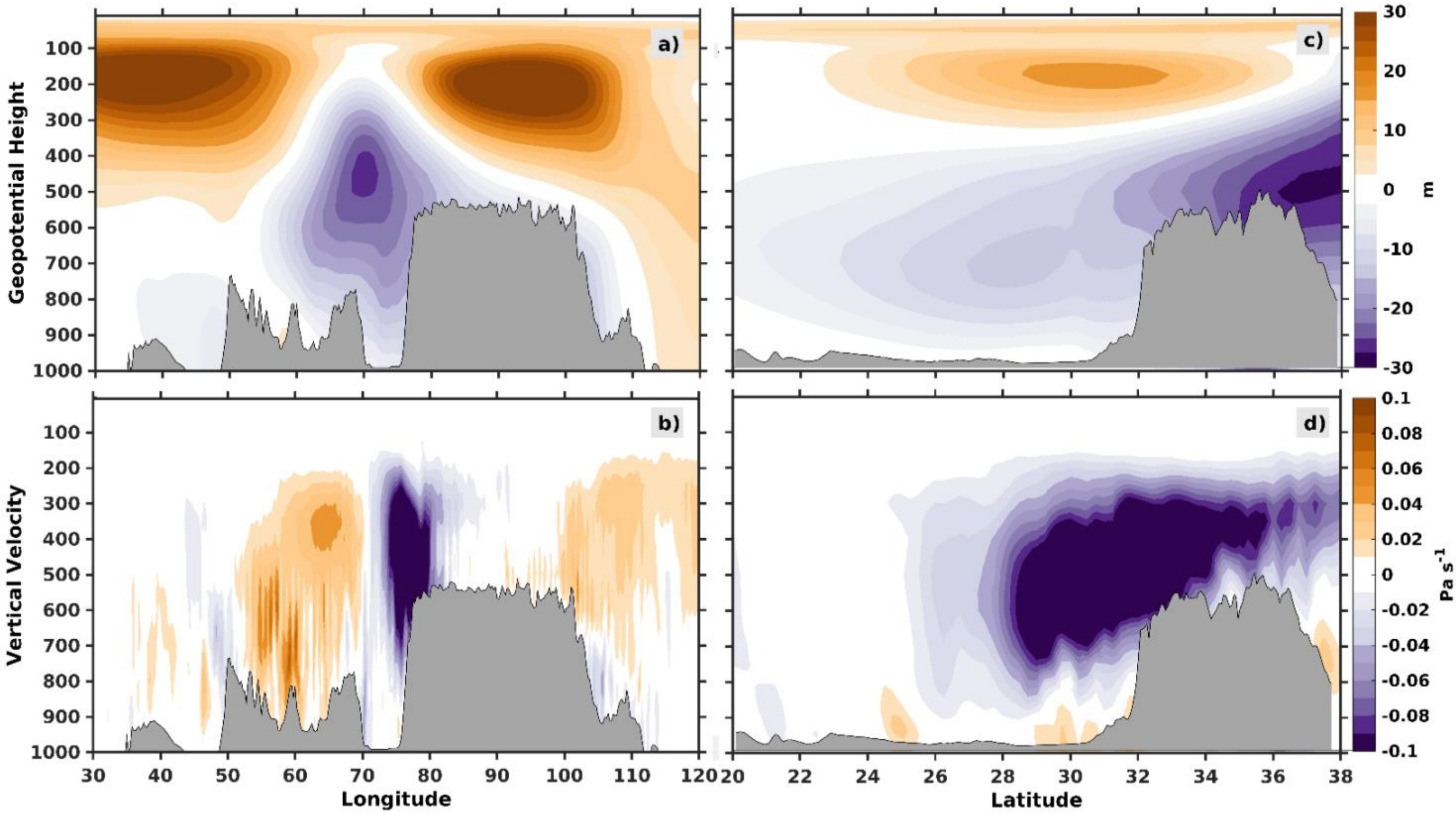

Figure 4: Composite vertical-meridional cross-sections of the anomalies of (a) geopotential height and (b) vertical velocity along 28°N–35°N for ISM extreme precipitation events occurring over Himalayas. Plots (c, d) represents vertical-zonal cross-sections of the anomalies of geopotential height and vertical velocity respectively along the 72°E–82°E.

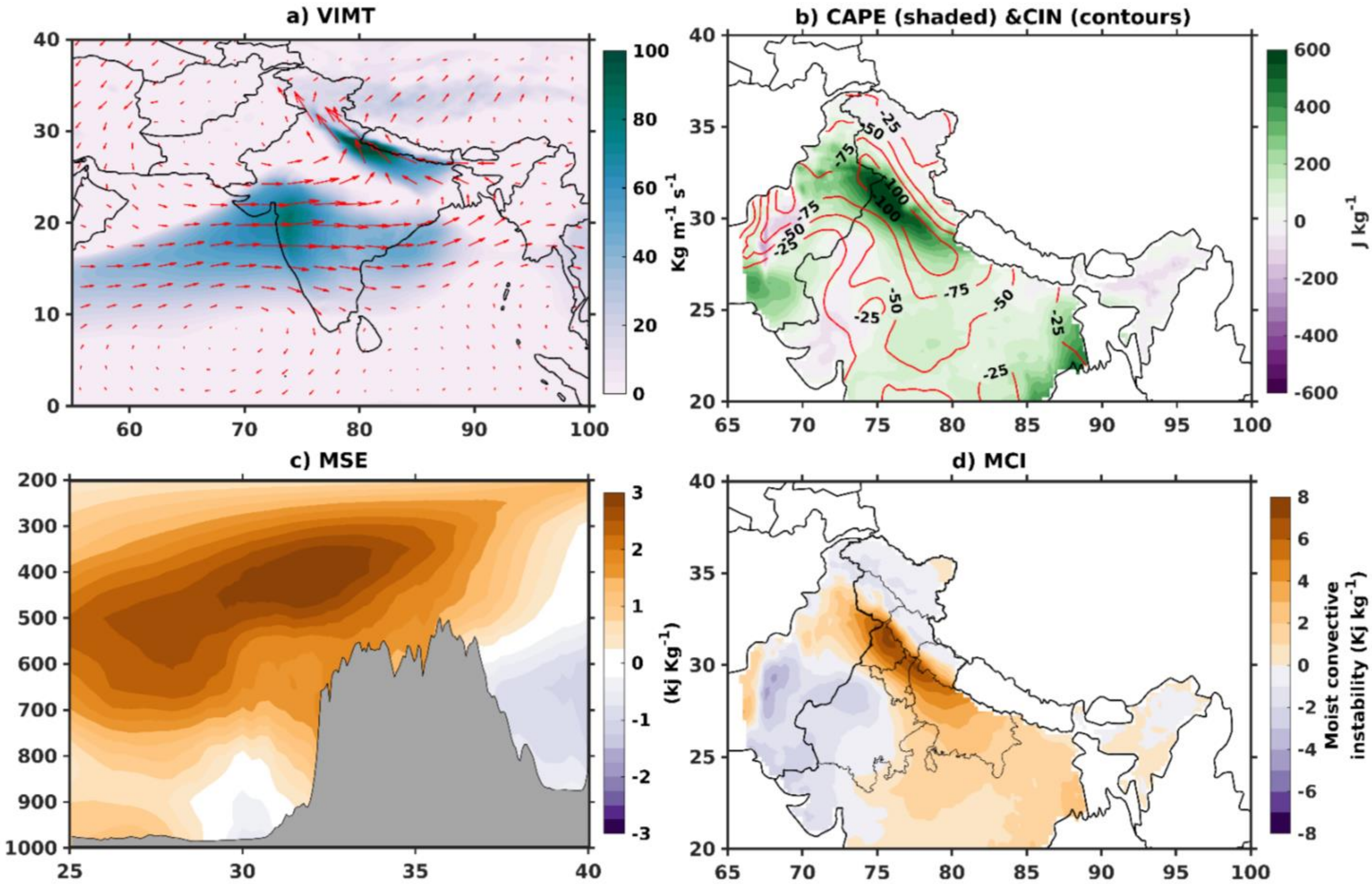

Figure 5: a) Composites of vertically integrated moisture transport (Kg m^{-1} s^{-1}) during EPEs over Himalayas. b) shows the convective available potential energy (shaded) and convective inhibition (contours). C) represents the composite of vertical-zonal cross-sections anomalies of moist static energy, and c) shows the moist convective instability during summer monsoon EPEs.

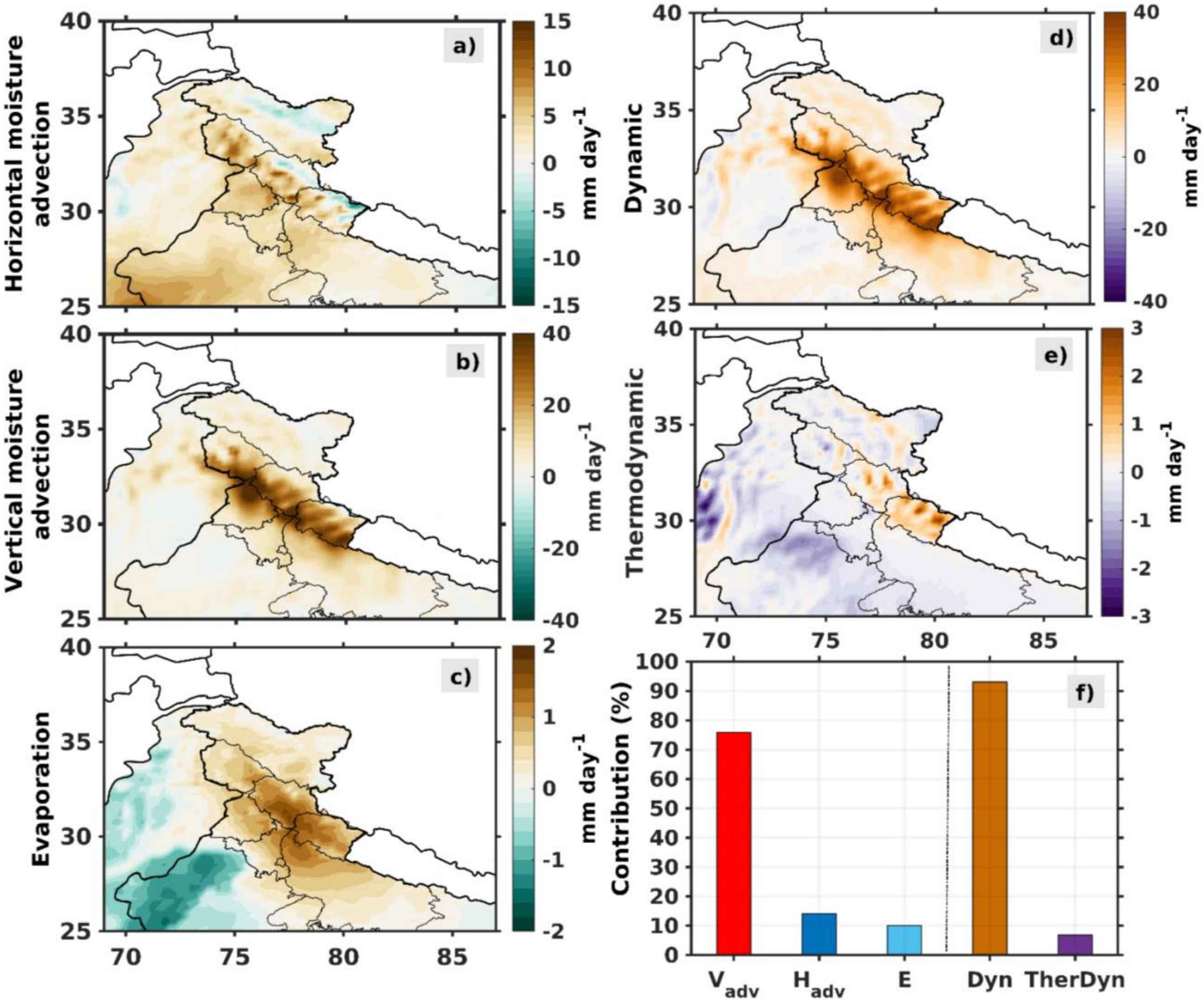

Figure 6. Composite anomalies of moisture-budget components during the EPEs over Himalayas. (a) Horizontal moisture advection, (b) Vertical moisture advection, (c) Surface evaporation (d) Dynamic component, and (e) thermodynamic component of vertical advection term over Himalayas during ISM extremes. f) represent contributions of moisture budget components spatially aggregated over the foothills of Himalayas as indicated in Figure. 2a.

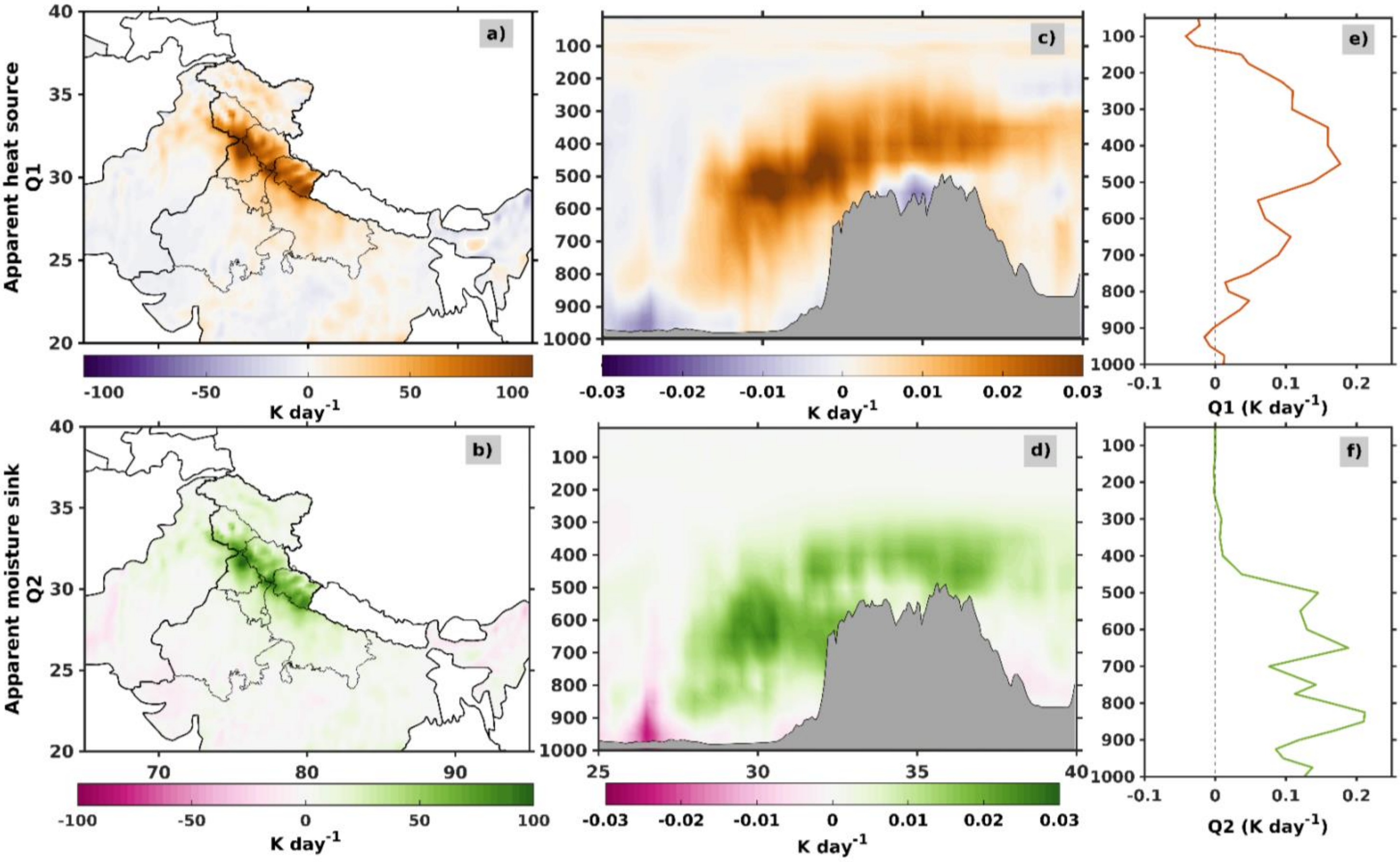

Figure 7. The spatial distribution of composites of a) apparent heat source (Q1), and b) moisture sink (Q2) during summer monsoon EPEs over Himalayas. Figure (c) and (d) represent the vertical cross section of composite of Q1 and Q2 respectively. Area average vertical structure of composite of the apparent heat source, and moisture sink over the HFB are shown in (e, f) respectively.

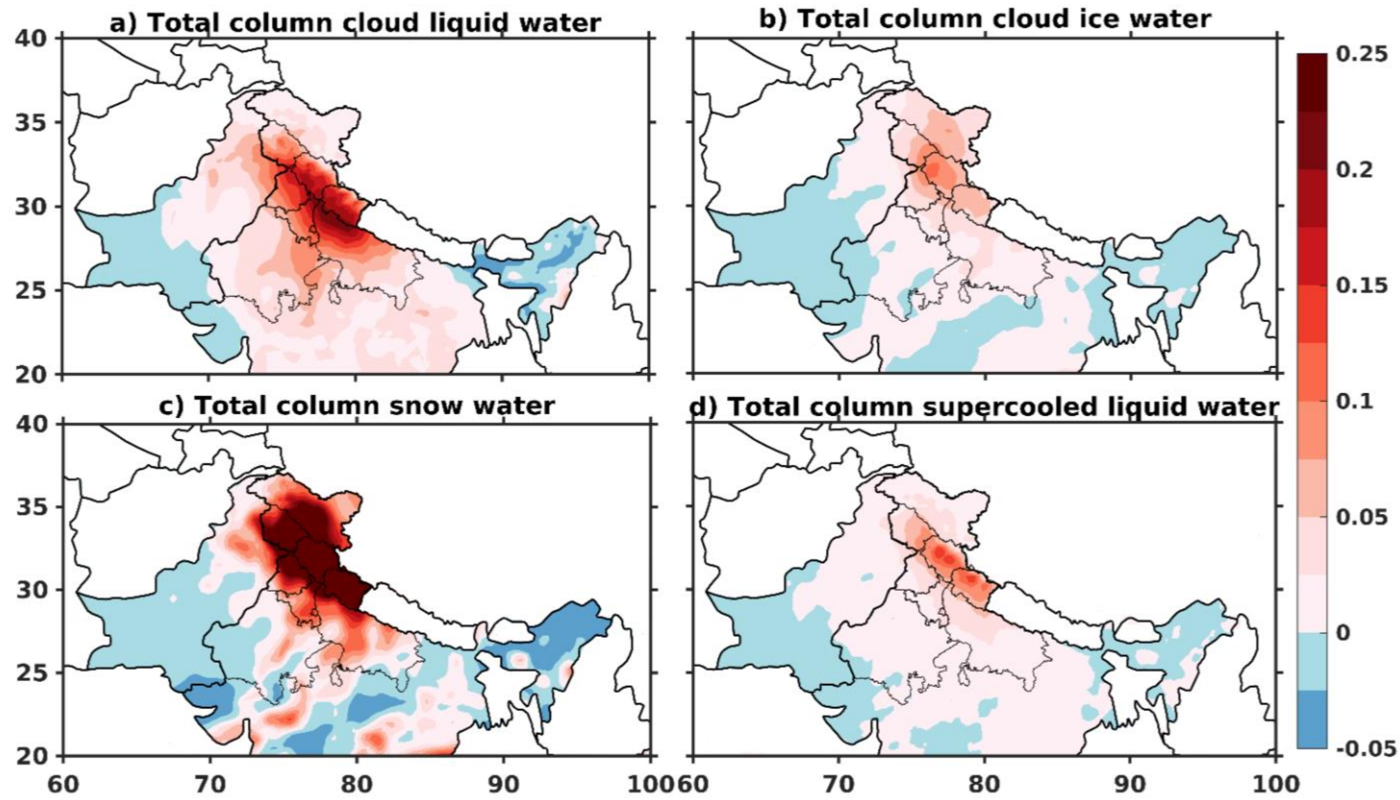

Figure 8: Composites of total column of hydrometeors a) total column cloud liquid water b) total column cloud ice water c) total column snow water d) total column supercooled liquid water during summer monsoon EPEs over Himalayas.

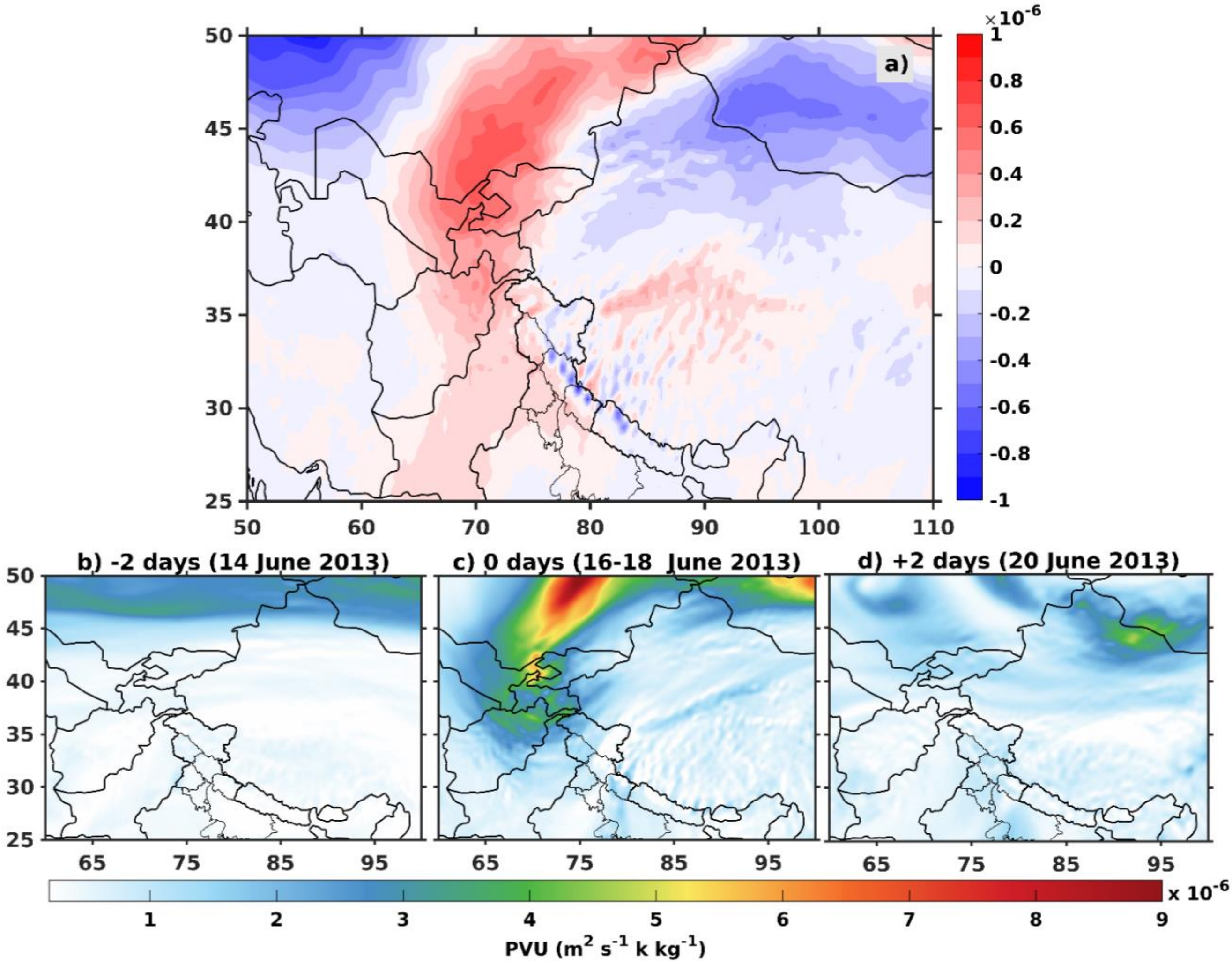

Figure 9: A composite map of Ertel potential vorticity (×10^{-6} PVU) on 330 K isentropic surface during ISM extreme precipitation events. (b) represent two days before (14 June 2013) the extreme precipitation Ertel potential vorticity (×10^{-6} PVU) on 330 K isentropic surface for Kedarnath flood 16-18 June 2013. (c) shows during extreme precipitation days (16-18) June 2013 and, (c) represents two days after (20 June 2013) the extreme precipitation day for Kedarnath flood.

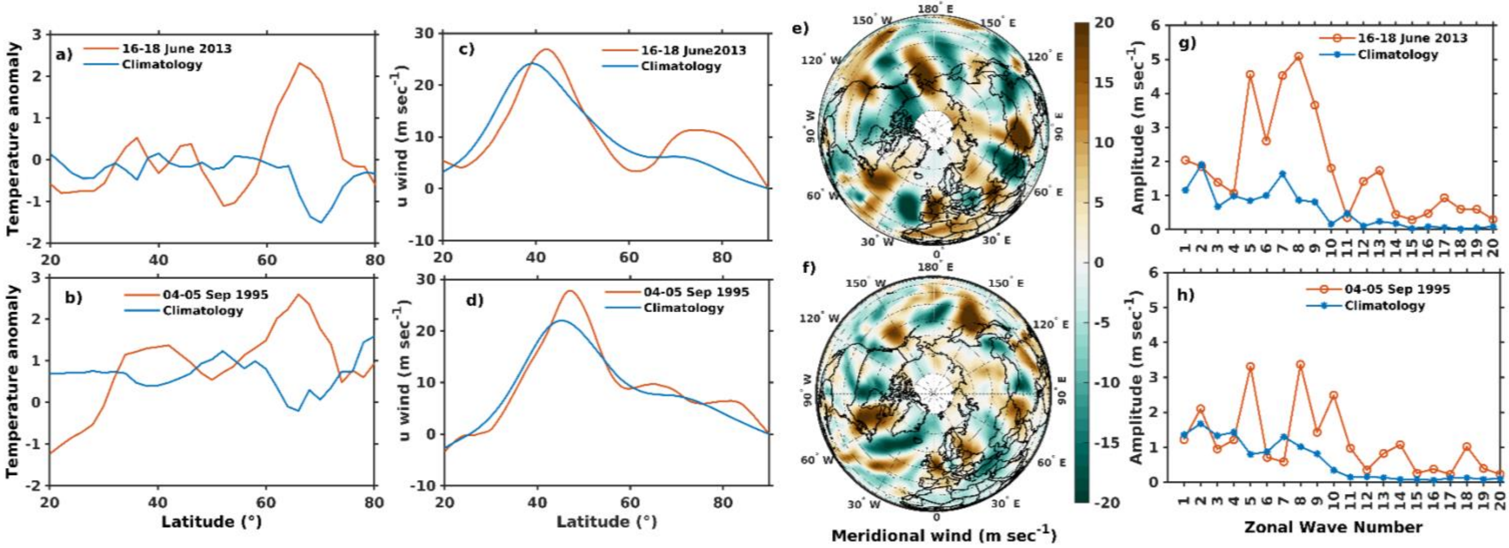

Figure 10: Meridional 2-meter air temperature anomalies averaged over the region 20°N to 80°N during extreme precipitation days (16-18) June 2013, and 04-05 September 1995 extreme rainfall event shown (a, b) respectively. The blue line indicates the anomaly for the extreme event, and the red line shows the climatology of these event days (1979–2020). (c, d) zonal wind profiles associated average over (25°N to 65°N) with extreme events. (e, f) represents the upper-troposphere (200hPa) meridional wind fields over Northern Hemisphere, and subplots (g) and (h) show the zonal wave number spectra for the meridional wind fields at 200hPa over 27° to 60°N during the extreme precipitation days in 16-18 June 2013 and 04-05 September 1995, respectively.

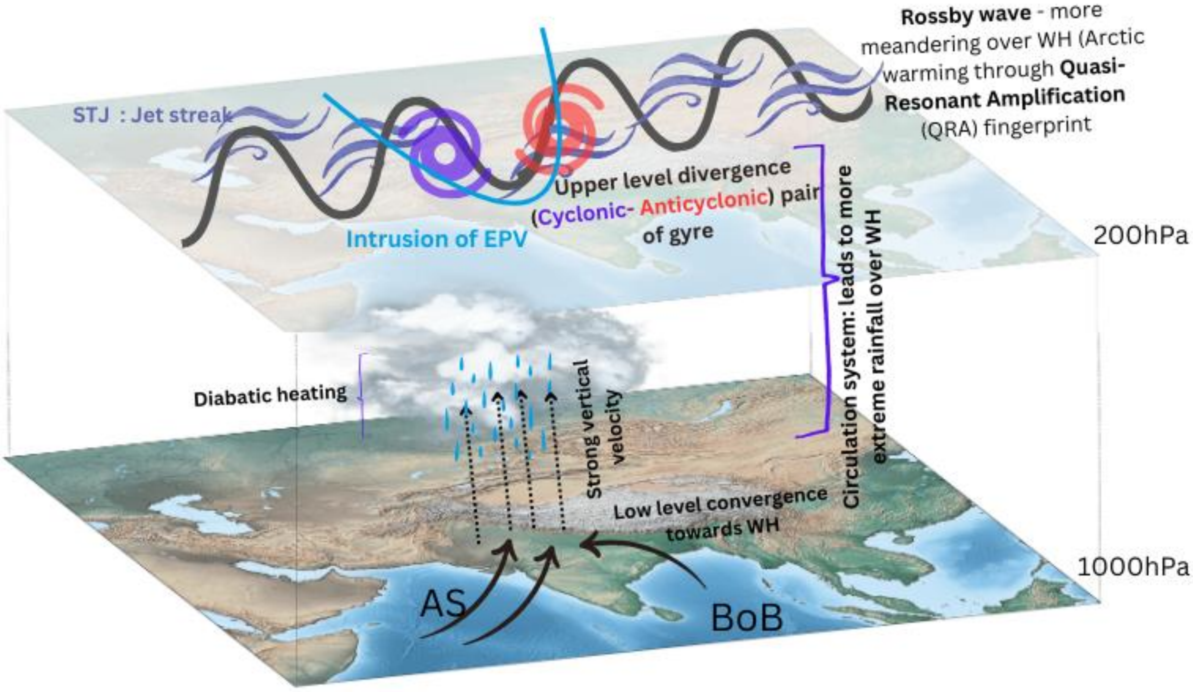

Figure 11: Proposed mechanism of EPEs over the Himalayas during ISM